J. Fluid Mech. (2020), *vol.* 883, A36. © Cambridge University Press 2019
doi:10.1017/jfm.2019.898

Velocity-defect laws, log law and logarithmic friction law in the convective atmospheric boundary layer

Chenning Tong[1,†] **and Mengjie Ding**[1]

[1]Department of Mechanical Engineering, Clemson University, Clemson, SC 29634, USA

(Received 26 December 2018; revised 5 September 2019; accepted 24 October 2019)

The mean velocity profile in the convective atmospheric boundary layer (CBL) is derived analytically. The shear-stress budget equations and the mean momentum equations are employed in the derivation. The multi-point Monin–Obukhov similarity (MMO) recently proposed and analytically derived by Tong & Nguyen (*J. Atmos. Sci.*, vol. 72, 2015, pp. 4337–4348) and Tong & Ding (*J. Fluid Mech.*, vol. 864, 2019, pp. 640–669) provides the scaling properties of the statistics in the shear-stress budget equations. Our previous and present studies have shown that the CBL is mathematically a singular perturbation problem. Therefore, we obtain the mean velocity profile using the method of matched asymptotic expansions. Three scaling layers are identified: the outer layer, which includes the mixed layer, the inner-outer layer and the inner-inner layer, which includes the roughness layer. There are two overlapping layers, the local-free-convection layer and the log layer, respectively. Two new velocity-defect laws are discovered: the mixed-layer velocity-defect law and the surface-layer velocity-defect law. The local-free-convection mean profile is obtained by asymptotically matching the expansions in the first two layers. The log law is obtained by matching the expansions in the last two layers. The von Kármán constant is obtained using velocity and length scales, and therefore has a physical interpretation. A new friction law, the convective logarithmic friction law, is obtained. The present work provides an analytical derivation of the mean velocity profile hypothesized in the Monin–Obukhov similarity theory, and is part of a comprehensive derivation of the MMO scaling from first principles.

Key words: boundary layer structure, atmospheric flows, turbulent boundary layers

1. Introduction

The mean velocity profile is one of the most important properties of a turbulent boundary layer. The classical high-Reynolds-number (neutral) boundary layer over a smooth plane has a two layer structure. In the thin layer close to the wall viscous effects are important, leading to the law of the wall (Prandtl 1925). In the layer away from the wall, the velocity-defect law was obtained (von Kármán 1930). The log law was obtained for the overlapping region of the two layers (von Kármán 1930).

† Email address for correspondence: ctong@clemson.edu

Furthermore, the logarithmic friction law was obtained from the log law and the velocity-defect law (Millikan 1938).

For the convective atmospheric boundary layer (CBL), the Monin–Obukhov similarity theory (MOST) (Obukhov 1946; Monin & Obukhov 1954) predicts that the non-dimensional mean shear in the surface-layer scales as $\phi_m(-z/L)$, where $L = -u_*^3/(\kappa(g/\Theta)Q)$, with z, L, u_*, κ, g, Θ and Q the distance from the surface, the Obukhov length, the friction velocity, the von Kármán constant, the gravity acceleration, the mean potential temperature, and the surface temperature flux, respectively. For $-z/L \ll 1$, $\phi_m = 1$, the theory is consistent with the log law, which has been confirmed by numerous measurements and simulations (e.g. Businger *et al.* 1971; Wyngaard, Coté & Izumi 1971). The physical justification for the existence of the log law in the presence of the convective eddies is based on the concepts of attached eddies and inactive motions (Townsend 1976), and therefore appears to be less rigorous compared with that for the neutral boundary layer. In the local-free-convection layer ($-z/L \gg 1$ but $z/z_i \ll 1$), the non-dimensional mean shear has been implied to vary as $(-z/L)^{-4/3}$ (Monin & Obukhov 1954; Wyngaard *et al.* 1971), where z_i is the boundary layer (inversion) height.

The velocity-defect law for the neutral atmospheric boundary layer (ABL) was proposed for the difference between the outer layer mean velocity and the geostrophic wind, U_g, with u_* as the velocity scale (Blackadar & Tennekes 1968). Garratt, Wyngaard & Francey (1982) analysed the velocity defect in the CBL with u_* as the velocity scale. A geostrophic drag law was also proposed (Lettau 1959; Kazanski & Monin 1960; Csanady 1967; Blackadar & Tennekes 1968; Brown 1973). Zilitinkevich, Laikhtman & Monin (1967) and Zilitinkevich (1969) extended the geostrophic drag law to include buoyancy effects,

$$\frac{U_g}{u_*} = \frac{1}{\kappa}\ln\frac{h}{h_0} + A\left(\frac{h}{L}\right), \tag{1.1}$$

where $h = u_*/f$ and h_0 are the Ekman layer height and the roughness height, respectively. However, this drag law is not supported by measurements (Zilitinkevich & Chalikov 1968; Clarke 1970*a*,*b*, 1972). Arya (1975) replaced u_*/f by the inversion height z_i. Garratt *et al.* (1982) proposed a three layer model, which led to a drag law that uses the Monin–Obukhov stability function (2.102). There appears to be systematic deviations of the drag law from observations (Garratt *et al.* 1982).

Zilitinkevich & Deardorff (1974) proposed a velocity-defect law with a velocity scale of u_* and used it to match the log law to obtain a resistance law for the CBL. Zilitinkevich (1975) and Zilitinkevich, Fedorovich & Shabalova (1992) proposed another velocity-defect law with a velocity scale $u_*(u_*/w_*)$ and matched it to an approximate velocity profile in the local-free-convection layer to obtain another resistance law, where w_* is the mixed-layer velocity (or Deardorff) scale. In both cases, the streamwise geostrophic wind component is used and only a single velocity defect is assumed for the entire CBL and therefore cannot properly represent the defects in the CBL.

In the present work we derive the mean velocity profile in the CBL from first principles (the profile obtained previously is not based on first principles). The mean momentum equations and the shear-stress budget equations, which contain the mean shear, are employed in the derivation. The scaling properties of some of the statistics in these equations are needed for the derivation. Because MOST does not correctly predict the scaling of all the statistics in the surface layer, it cannot provide the

definitive scaling properties needed. Instead, these scaling properties can be derived analytically from the multi-point Monin–Obukhov similarity theory (MMO) (Tong & Nguyen 2015, Tong & Ding 2019).

The Monin–Obukhov similarity theory is the foundation for understanding the atmospheric surface layer, and has been successfully used to scale many single-point surface layer statistics (e.g. Businger *et al.* 1971, Wyngaard & Coté 1971, Wyngaard *et al.* 1971, Kaimal *et al.* 1972, Kaimal 1978). However, it has been known, perhaps since the late 1950s, that some very important class of statistics do not scale according to MOST (e.g. Lumley & Panofsky 1964; Kaimal *et al.* 1972; Kaimal 1978; Caughey & Palmer 1979), resulting in incomplete surface-layer similarity and raising questions on the existence of complete surface-layer similarity. To resolve this long-standing issue, MMO, was recently proposed (Tong & Nguyen 2015) as a generalization of MOST, hypothesizing that multi-point statistics have universal complete surface-layer similarity, i.e. all multi-point statistics have universal surface-layer scaling (Tong & Ding 2019). Thus MMO is a general surface-layer similarity theory, and universal complete surface-layer scaling properties can be obtained from MMO.

Similar to MOST, MMO was also proposed as hypotheses. Measurements and simulations can only provide supporting evidence, but not a proof. To provide analytical support to MMO, we have recently begun deriving the MMO similarity properties for some of the important statistics from first principles. Tong & Ding (2019) have derived the MMO scaling of the horizontal Fourier transforms of the velocity and potential temperature.

The similarity properties of one-point statistics, hypothesized in MOST, can also be derived using MMO. For example, variances can in principle be obtained by integrating the spectra, which follow the MMO scaling. The profiles of the vertical velocity and potential temperature variances have been derived using MMO and the method of asymptotic expansions (Tong & Ding 2018). On the other hand, the mean fields, such as the mean velocity and potential temperature profiles, cannot be obtained directly by reducing the multi-point statistics of the fluctuating variables. Their derivation requires the use of the budget equations for the mean shear stress and temperature fluxes. To this end, the CBL has previously been shown to be mathematically a singular perturbation problem with one outer layer and two inner layers (e.g. Tong & Ding 2019). Thus we derive the mean velocity profile using the method of matched asymptotic expansions. Therefore, the derivation in the present study is part of the comprehensive derivation of the scaling properties using MMO.

The capping inversion layer also has a different scaling than does both the outer and inner layers that we consider, and therefore is beyond the derivation based on the Monin–Obukhov similarity (both MOST and MMO). In the present study we only consider the profiles below the inversion layer. Furthermore, since the Monin–Obukhov similarity applies to the surface layer, in a boundary layer that obeys this similarity, the absolute value of the Obukhov length must be within the surface layer. Therefore we only consider the convective boundary layer with $-L \ll z_i$.

In the following, we will derive the mean velocity profile for the convective atmospheric boundary layer (§ 2). Although the derivation is for a rough wall, the derivation can easily be extended to the case with a smooth wall. Comparisons of the profiles with large-eddy simulation (LES) are given in § 3, followed by the conclusions.

2. Mean velocity profile using matched asymptotic expansions

We consider a horizontally homogeneous barotropic atmospheric convective boundary layer with geostrophic velocity components U_g and V_g, capped by a

temperature inversion. The x-direction of the coordinate system is aligned with the mean velocity direction in the bulk of the mixed-layer (it is shown later in this section that the variations of the mean wind direction in the mixed layer are small for the CBL considered). The shear-stress budget equations and the mean momentum equations are

$$\frac{\partial \overline{uw}}{\partial t} + \overline{w^2}\frac{\partial U}{\partial z} - \frac{g}{T}\overline{u\theta} + \frac{\partial \overline{uw^2}}{\partial z} + \overline{w\frac{\partial p}{\partial x}} + \overline{u\frac{\partial p}{\partial z}} + 2(\Omega_2\overline{w^2} + \Omega_1\overline{uv} - \Omega_3\overline{vw} - \Omega_2\overline{u^2}) = 0, \tag{2.1}$$

$$\frac{\partial \overline{vw}}{\partial t} + \overline{w^2}\frac{\partial V}{\partial z} - \frac{g}{T}\overline{v\theta} + \frac{\partial \overline{vw^2}}{\partial z} + \overline{w\frac{\partial p}{\partial y}} + \overline{v\frac{\partial p}{\partial z}} + 2(\Omega_1\overline{v^2} + \Omega_3\overline{uw} - \Omega_1\overline{w^2} - \Omega_2\overline{uv}) = 0, \tag{2.2}$$

$$\frac{\partial V}{\partial t} + \frac{\partial \overline{vw}}{\partial z} = f(U_g - U) + \frac{\mathrm{d}\tau_{ry}}{\mathrm{d}z}, \tag{2.3}$$

$$\frac{\partial U}{\partial t} + \frac{\partial \overline{uw}}{\partial z} = f(V - V_g) + \frac{\mathrm{d}\tau_{rx}}{\mathrm{d}z}, \tag{2.4}$$

where Ω_i, $f = 2\Omega_3$, τ_{rx} and τ_{ry} are the components of Earth's rotation vector, Coriolis parameter, and the shear-stress in the x- and y-directions induced by the surface roughness, respectively. The Coriolis terms in (2.1) and (2.2) are of higher order (e.g. Wyngaard 2010), thus we neglect them in this analysis.

Similar to the classical neutral boundary layer (e.g. Millikan 1938, Panton 2005), equations (2.1) to (2.4) for the convective surface layer also form a singular perturbation problem, but with a three layer structure, which we analyse in the following using the method of matched asymptotic expansions. A schematic of the structure obtained in the analysis is shown in figure 1.

In the outer layer, analysed in § 2.1, turbulent fluctuations are dominated by buoyancy effects. The larger vertical velocity variance reduces the mean velocity gradient compared to a neutral boundary layer. The outer layer is affected by the external influences (from above), and therefore is not universal. The scales in this layer include a mixed-layer mean velocity scale, the lateral geostrophic wind component, the surface kinematic stress (u_*^2), the surface temperature flux (Q), the inversion height (z_i), the mixed-layer velocity scale (w_*) and a lateral stress scale (2.5). A new velocity-defect law, the mixed-layer velocity-defect law, is derived, which has a velocity scale of $u_*(u_*/w_*)$. The inner-outer layer is characterized by the importance of both buoyancy and shear production (§ 2.2). In this layer, the terms in (2.1) to (2.4) are isolated from the external influences, and therefore are universal. The scales for this layer are the mixed-layer mean velocity scale, the lateral geostrophic wind component, the surface stress and temperature flux, the Obukhov length (L), and a lateral stress scale. Another new velocity-defect law, the surface-layer velocity-defect law is derived, which has a velocity scale of u_*. The overlapping portion of the outer and inner-outer layers is the local-free-convection layer (§ 2.3). The inner-inner layer is characterized by negligible buoyancy production of the turbulent fluctuations (§ 2.4), with the shear production and roughness effects being important. Similar to the inner-outer layer, this layer is also universal. Its scales are the roughness height, the surface stress and the surface temperature flux. The overlapping portion of the inner-outer layer and inner-inner layer is the log layer. A new logarithmic friction law (§ 2.5), the convective logarithmic friction law is derived by combining the log law and the surface-layer velocity-defect law.

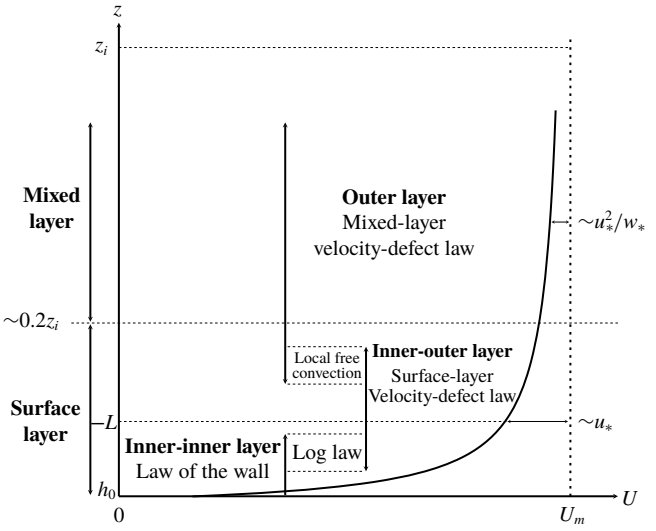

FIGURE 1. Schematic of the overall CBL mean velocity profile, which has a three layer structure. In the outer and inner-outer layers, the mean velocity follows the mixed-layer and surface-layer velocity-defect laws, respectively. In the inner-inner layer, it obeys the law of the wall (only up to $z < -L$, however).

2.1. *The outer expansions*

The outer layer in the asymptotic expansions is defined as the layer with z being of the order of z_i, but below the capping inversion. We use U_m, V_g, z_i, u_*^2, $u_*^2 w_e/(fz_i) = -V_g w_e$, w_*^2, Q and z_i/w_* as the outer scales for the mean velocity components, height from the surface, the streamwise and lateral kinematic stress components, velocity variance, potential temperature flux, and time to define the dimensionless outer variables (with a subscript $_o$),

$$\left.\begin{gathered} U(z) = U_m U_o\left(\frac{z}{z_i}\right), \quad V(z) = V_g V_o\left(\frac{z}{z_i}\right), \quad \overline{uw} = u_*^2 \overline{uw}_o, \quad \overline{vw} = \frac{u_*^2 w_e}{fz_i}\overline{vw}_o, \\ z = z_i z_o, \quad \overline{u\theta} = Q\overline{u\theta}_o, \quad t = \frac{z_i}{w_*}\tau, \quad \overline{w^2} = w_*^2\overline{w_o^2}, \end{gathered}\right\} \tag{2.5}$$

where w_e is the entrainment velocity (at the capping inversion). These outer scales are given by the geometry (z_i), the external parameters (f, w_e), and the boundary conditions (U_g, Q and u_*, although u_* is not an independent one) of the problem. The scale of $\overline{vw}$ reflects the balance between the lateral pressure gradient and the lateral stress generated by entrainment (Lilly 1968; Deardorff 1973; Wyngaard 2010). The mixed-layer scale is obtained from Q, z_i and g/Θ, and is also an external parameter, because it is not a parameter in MOST or MMO. The scale of lateral stress and V_g are obtained with the lateral mean velocity being of higher order in the outer layer. The outer-layer mean velocity scale U_m will be determined later in this section (2.26), but is asymptotically close to the mean velocity in the mixed layer. Panton (2005) showed that the use of the free-stream velocity as the velocity scale leads to the velocity-defect law in neutral boundary layers. In the present study, the use of U_m also leads to velocity-defect laws in the CBL.

These parameters (outer scales) and the budget equations (2.1)–(2.4) form the singular perturbation problem that describes the mean velocity of the CBL. In the following, the scaling laws of the mean velocity will be derived by analysing this problem using the method of matched asymptotic expansions. Therefore, our analysis is based on first principles. These scaling laws could potentially also be obtained less rigorously using dimensional analysis without involving first principles (the budget equations).

Writing equations (2.1) and (2.2) in terms of the outer variables,

$$\frac{\partial \overline{uw}_o}{\partial \tau}\frac{u_*^2 w_*}{z_i} + w_*^2\overline{w_o^2}\frac{U_m}{z_i}\frac{\partial U_o}{\partial z_o} - \frac{g}{T}Q\overline{u\theta}_o + \frac{w_* u_*^2}{z_i}\left(\frac{\partial \overline{uw^2}_o}{\partial z_o} + \left(\overline{w\frac{\partial p}{\partial x}}\right)_o + \left(\overline{u\frac{\partial p}{\partial z}}\right)_o\right) = 0, \tag{2.6}$$

$$\frac{\partial \overline{vw}_o}{\partial \tau}\frac{u_*^2 w_e}{f z_i}\frac{w_*}{z_i} + w_*^2\overline{w_o^2}\frac{V_g}{z_i}\frac{\partial V_o}{\partial z_o} - \frac{g}{T}Q\overline{v\theta}_o + \frac{w_*}{z_i}\frac{u_*^2 w_e}{f z_i}\left(\frac{\partial \overline{vw^2}_o}{\partial z_o} + \left(\overline{w\frac{\partial p}{\partial y}}\right)_o + \left(\overline{v\frac{\partial p}{\partial z}}\right)_o\right) = 0, \tag{2.7}$$

and dividing them by $w_*^2 U_m/z_i$ results in the non-dimensional shear-stress budget equations for the outer variables,

$$\frac{u_*}{w_*}\frac{u_*}{U_m}\frac{\partial \overline{uw}_o}{\partial \tau} + \overline{w_o^2}\frac{\partial U_o}{\partial z_o} - \frac{w_*}{U_m}\overline{u\theta}_o + \frac{u_*}{w_*}\frac{u_*}{U_m}\left(\frac{\partial \overline{uw^2}_o}{\partial z_o} + \left(\overline{w\frac{\partial p}{\partial x}}\right)_o + \left(\overline{u\frac{\partial p}{\partial z}}\right)_o\right) = 0, \tag{2.8}$$

$$\frac{w_e}{w_*}\frac{V_g}{U_m}\frac{\partial \overline{vw}_o}{\partial \tau} + \overline{w_o^2}\frac{V_g}{U_m}\frac{\partial V_o}{\partial z_o} - \frac{w_*}{U_m}\overline{v\theta}_o + \frac{w_e}{w_*}\frac{V_g}{U_m}\left(\frac{\partial \overline{vw^2}_o}{\partial z_o} + \left(\overline{w\frac{\partial p}{\partial y}}\right)_o + \left(\overline{v\frac{\partial p}{\partial z}}\right)_o\right) = 0. \tag{2.9}$$

There are two independent small parameters $(u_*/w_*)(u_*/U_m)$ and $(w_e/w_*)(V_g/U_m)$ in (2.8) and (2.9), since in a CBL that obeys the Monin–Obukhov similarity $u_* \ll w_*$, $u_* \ll U_m$, $w_e \ll w_*$ and $V_g < U_m$. The streamwise temperature flux in the buoyancy term in (2.8) scales as $(-z/L)^{-2/3}$ in the local-free-convection layer (Wyngaard *et al.* 1971), and is smaller in the outer layer as the turbulence becomes increasingly horizontally isotropic. The cross-wind temperature flux is much smaller. Therefore, the buoyancy terms are smaller than the terms containing $(u_*/w_*)(u_*/U_m)$ and $(w_e/w_*)(V_g/U_m)$. These small parameters are a result of the outer scales (2.5) and the terms in (2.8) and (2.9), reflecting the physics of the CBL. Therefore, in general, we can write the outer expansions for U and V as,

$$U_o(z_o) = U_{o,1}(z_o) + \frac{u_*}{w_*}\frac{u_*}{U_m}U_{o,2a}(z_o) + \frac{w_e}{w_*}\frac{V_g}{U_m}U_{o,2b}(z_o), \tag{2.10}$$

$$\frac{V_g}{U_m}V_o(z_o) = \frac{V_g}{U_m}V_{o,1}(z_o) + \frac{u_*}{w_*}\frac{u_*}{U_m}V_{o,2a}(z_o) + \frac{w_e}{w_*}\frac{V_g}{U_m}V_{o,2b}(z_o). \tag{2.11}$$

Thus,

$$V_o(z_o) = V_{o,1}(z_o) - \frac{fz_i}{w_*} V_{o,2a}(z_o) + \frac{w_e}{w_*} V_{o,2b}(z_o). \tag{2.12}$$

The last terms in the outer expansions result from the Coriolis effects. The expansions for the velocity derivatives are

$$\frac{\partial U_o}{\partial z_o} = \frac{\partial U_{o,1}}{\partial z_o} + \frac{u_*}{w_*}\frac{u_*}{U_m}\frac{\partial U_{o,2a}}{\partial z_o} + \frac{w_e}{w_*}\frac{V_g}{U_m}\frac{\partial U_{o,2b}}{\partial z_o}, \tag{2.13}$$

$$\frac{\partial V_o}{\partial z_o} = \frac{\partial V_{o,1}}{\partial z_o} - \frac{fz_i}{w_*}\frac{\partial V_{o,2a}}{\partial z_o} + \frac{w_e}{w_*}\frac{\partial V_{o,2b}}{\partial z_o}. \tag{2.14}$$

Inserting equations (2.13) and (2.14) into (2.8) and (2.9), we find that the only leading-order terms are the mean-shear production terms (those that do not contain small parameters). Thus,

$$\frac{\partial U_{o,1}}{\partial z_o} = 0, \quad \frac{\partial V_{o,1}}{\partial z_o} = 0, \tag{2.15a,b}$$

resulting in

$$U_{o,1} = 1, \tag{2.16}$$

$$V_{o,1} = 0, \quad \text{since } V = 0 \text{ at some height in the mixed layer.} \tag{2.17}$$

Setting the leading order U to U_m results in $U_{o,1} = 1$. Thus, from the outer expansions (2.10) and (2.12), we have

$$U = U_m U_o = U_m + \frac{u_*}{w_*} u_* U_{o,2a} + \frac{w_e}{w_*} V_g U_{o,2b}, \tag{2.18}$$

$$V = V_g V_o = \frac{u_*}{w_*} u_* V_{o,2a} + \frac{w_e}{w_*} V_g V_{o,2b}. \tag{2.19}$$

The leading-order expansions (2.16) and (2.17) are not valid in the roughness layer, confirming that the system described by (2.8) and (2.9) is a singular perturbation problem. The second-order terms for U

$$U - U_m = \frac{u_*}{w_*} u_* U_{o,2a} + \frac{w_e}{w_*} V_g U_{o,2b} \tag{2.20}$$

are the difference between the mean velocity and U_m. Inserting $\partial U_o/\partial z_o$ (2.13) into (2.8) leads to $\partial U_{o,2b}/\partial z_o = 0$, since at the second order, equation (2.8) does not contain the parameter $(w_e/w_*)(V_g/U_m)$ (§ 2.3 further shows that $U_{o,2b} = 0$). Equation (2.20) is a new velocity-defect law, which we term the mixed-layer velocity-defect law. The scale of the defect is $u_*(u_*/w_*)$, which is asymptotically smaller than that in a neutral boundary layer (u_*). Physically this is because the larger vertical velocity variance ($\sim w_*^2$) reduces the mean shear to maintain the same shear stress. Some previous works (e.g. Zilitinkevich & Deardorff 1974, Garratt *et al.* 1982) defined the velocity defect as $U - U_g$, which also depends on w_e and f as discussed later in this subsection. With such a definition, the variations of U in the outer layer, which is asymptotically smaller than $U - U_g$, is obscured. Consequently, this definition does not reflect the velocity defect in the outer layer.

The new velocity-defect law further indicates the importance of the mixed-layer mean velocity scale U_m. This defect law provides the scaling of the variations of the mean velocity in the mixed layer, and therefore is different in nature from that of Garratt *et al.* (1982), which describes the difference between the height-averaged mean velocity and the geostrophic wind.

Similarly, inserting $\partial V_o/\partial z_o$ (2.14) into (2.9) leads to $\partial V_{o,2a}/\partial z_o = 0$; since at the second order, equation (2.9) does not contain the parameter fz_i/w_* (§ 2.3 further shows that $V_{o,2a} = 0$). We can evaluate the magnitudes of V for typical values of w_*, w_e and V_g using (2.19) as

$$V \sim \frac{w_e}{w_*} V_g \sim \frac{0.03}{2.0} \times 1 \sim 0.01 \text{ m s}^{-1}. \tag{2.21}$$

Thus, the change in the direction of the mean velocity in the outer layer is negligible compared to that across the inversion layer ($\sim 11^\circ$ for $U_g = 5$ m s^{-1} and $V_g = 1$ m s^{-1}).

The equation for the second-order term $U_{o,2a}$ is,

$$\frac{\partial \overline{uw}_{o,1}}{\partial \tau} + \overline{w_{o,1}^2} \frac{\partial U_{o,2a}}{\partial z_o} - \frac{w_*^2}{u_*^2} \overline{u\theta}_{o,1} + \frac{\partial \overline{uw^2}_{o,1}}{\partial z_o} + \left(\overline{w \frac{\partial p}{\partial x}} \right)_o + \left(\overline{u \frac{\partial p}{\partial z}} \right)_o = 0. \tag{2.22}$$

This equation does not contain a small parameter (the buoyancy production term is also of order one as the horizontal flux is of order u_*^2/w_*^2). However, the scaling of $\overline{w_o^2}$ changes when z decreases to $z < -L$ (from u_f^2 to u_*^2, Tong & Ding 2018), also resulting in a non-uniformly valid solution and a singular perturbation problem, where $u_f = (\beta Q z)^{1/3}$ is the local-free-convection velocity scale. Although equation (2.22) is not explicitly used, it helps us identify the source of the singularity.

Given that the scale of $\overline{vw}$ is $u_*^2 w_e/(fz_i) = -V_g w_e$, we can write the mean momentum equation for V as,

$$V_g \frac{w_*}{z_i} \frac{\partial V_o}{\partial \tau} + \frac{u_*^2 w_e}{f z_i} \frac{1}{z_i} \frac{\partial \overline{vw}_o}{\partial z_o} = f U_m \frac{U_g - U}{U_m}. \tag{2.23}$$

Dividing this equation by $U_m w_*/z_i$ results in

$$\frac{V_g}{U_m} \frac{\partial V_o}{\partial \tau} + \frac{w_e}{w_*} \frac{V_g}{U_m} \frac{\partial \overline{vw}_o}{\partial z_o} = \frac{u_*}{V_g} \frac{u_*}{w_*} \left(\frac{U_g - U_m}{U_m} - \frac{u_*}{w_*} \frac{u_*}{U_m} U_{o,2a} \right). \tag{2.24}$$

For $z < z_i$, the mean velocity is quasi-steady, the time rate of change is dropped. Equation (2.23) becomes

$$\frac{\partial \overline{vw}_o}{\partial z_o} = \frac{U_g - U}{(u_*^2 w_e)/(f^2 z_i^2)}. \tag{2.25}$$

Both sides of (2.25) are of order one. It follows that $U_g - U_m$ scales as $u_*^2 w_e/(f^2 z_i^2)$, which is the jump in U across the inversion layer needed to balance the vertical derivative of the lateral stress in the outer layer. Thus, we can define the mean velocity scale U_m as

$$U_m \equiv U_g - \frac{u_*^2 w_e}{f^2 z_i^2}. \tag{2.26}$$

Garratt *et al.* (1982) obtained a similar expression for the height-averaged mixed-layer velocity. Thus,

$$\frac{\partial \overline{vw}_o}{\partial z_o} = \frac{U_g - U_m}{(u_*^2 w_e)/(f^2 z_i^2)} - \frac{(u_*/w_*)u_* U_{o,2a}}{(u_*^2 w_e)/(f^2 z_i^2)}, \\ = 1 - \frac{f^2 z_i^2}{w_* w_e} U_{o,2a}, \tag{2.27}$$

where,

$$\frac{f^2 z_i^2}{w_* w_e} \sim \frac{0.01}{2 \times 0.03} \sim 0.15. \tag{2.28}$$

Thus, there are small but significant variations of $\partial \overline{vw}_o/\partial z_o$ in the outer layer.

Using (2.19), the mean momentum equation for U can be written as

$$\frac{\partial \overline{uw}_o}{\partial z_o} = \frac{f z_i}{u_*^2}(V - V_g) = \frac{V_g - V}{V_g}, \\ = \frac{V_g - V}{U_m}\frac{U_m}{V_g} = 1 - \frac{w_e}{w_*}\frac{V_g}{U_m}\frac{U_m}{V_g} V_{o,2b}, \\ = 1 - \frac{w_e}{w_*} V_{o,2b}. \tag{2.29}$$

The parameter w_e/w_* is estimated as

$$\frac{w_e}{w_*} \sim \frac{0.03}{2} \sim 0.015, \tag{2.30}$$

indicating that the second-order terms on the right-hand side of (2.29) is of higher order, i.e. to the leading order, the $\overline{uw}_o$ varies linearly with z_o. Therefore the Coriolis term is of higher order and at the leading order, Earth's rotation does not affect the fundamental characteristics of the convective atmospheric boundary layer.

We note that if w_*^2 is used as the scale for the kinematic stress ($\overline{uw} = w_*^2 \overline{uw}_o$) to focus on the dynamics of $\overline{u_o^2}$ and $\overline{w_o^2}$, the non-dimensional shear-stress transport equation becomes,

$$\frac{\partial \overline{uw}_o}{\partial \tau} + \frac{U_m}{w_*}\overline{w_o^2}\frac{\partial U_o}{\partial z_o} - \overline{u\theta}_o + \frac{\partial \overline{uw^2}_o}{\partial z_o} + \left(\overline{w\frac{\partial p}{\partial x}}\right)_o + \left(\overline{u\frac{\partial p}{\partial z}}\right)_o = 0. \tag{2.31}$$

All the terms in this equation are of higher order, indicating that in the outer layer, the effects of the shear-stress dynamics on that of $\overline{u_o^2}$ and $\overline{w_o^2}$ are of higher order, whereas the leading budget terms in the equations of $\overline{u_o^2}$ and $\overline{w_o^2}$ are of order one (Tong & Ding 2018).

2.2. *The inner-outer expansion*

Two inner layers have been previously identified in the convective boundary layer (Tong & Ding 2018, 2019): one has a length scale of $-L$, which we term the inner-outer layer, and the other has a scale of h_0, which we term the inner-inner layer. This structure is in contrast with the neutral boundary layer, which has only one inner layer, and is a key difference between a convective boundary layer and a neutral one.

Tong & Ding (2018) have shown analytically using the budget equations for $\overline{w^2}$ and $\overline{\theta^2}$ that their scaling changes as z decreases across $-L$, going from buoyancy dominated to shear dominated. Therefore $-L$ and u_* are the length scale and vertical velocity scale, respectively. Accordingly, we define the dimensionless inner-outer variables as,

$$\left.\begin{aligned} U(z) = U_m U_{io}\left(-\frac{z}{L}\right), \quad V(z) = V_g V_{io}\left(-\frac{z}{L}\right), \quad \overline{uw} = u_*^2 \overline{uw}_{io}, \\ \overline{vw} = \frac{u_*^2 w_e}{f z_i}\left(-\frac{L}{z_i}\right)\overline{vw}_{io}, \quad z = -L z_{io}, \quad \overline{u\theta} = Q\overline{u\theta}_{io}, \quad \overline{w^2} = u_*^2 \overline{w^2_{io}}. \end{aligned}\right\} \tag{2.32}$$

The scale for $\overline{vw}$ is such because its gradient is of the same order of magnitude as in the outer layer ($U_g - U$ is constant to the leading order). Writing equations (2.1) and (2.2) in terms of the inner-outer variables,

$$\begin{aligned} &\frac{\partial \overline{uw}_{io}}{\partial \tau}\frac{u_*^2 w_*}{z_i} + u_*^2 \overline{w^2_{io}}\frac{U_m}{-L}\frac{\partial U_{io}}{\partial z_{io}} - \frac{g}{T}Q\overline{u\theta}_{io} \\ &\quad + \frac{u_*^3}{-L}\left(\frac{\partial \overline{uw^2}_{io}}{\partial z_{io}} + \left(\overline{w\frac{\partial p}{\partial x}}\right)_{io} + \left(\overline{u\frac{\partial p}{\partial z}}\right)_{io}\right) = 0, \end{aligned} \tag{2.33}$$

$$\begin{aligned} &\frac{\partial \overline{vw}_{io}}{\partial \tau}\frac{u_*^2 w_e}{f z_i}\left(-\frac{L}{z_i}\right)\frac{w_*}{z_i} + u_*^2 \overline{w^2_{io}}\frac{V_g}{-L}\frac{\partial V_{io}}{\partial z_{io}} - \frac{g}{T}Q\overline{v\theta}_{io} \\ &\quad + \frac{u_*}{z_i}\frac{u_*^2 w_e}{f z_i}\left(\frac{\partial \overline{vw^2}_{io}}{\partial z_{io}} + \left(\overline{w\frac{\partial p}{\partial y}}\right)_{io} + \left(\overline{v\frac{\partial p}{\partial z}}\right)_{io}\right) = 0, \end{aligned} \tag{2.34}$$

and dividing by $u_*^2 U_m/(-L)$ results in the non-dimensional shear-stress budget equations in the inner-outer layer,

$$\frac{u_*^2}{w_*^2}\frac{u_*}{U_m}\frac{\partial \overline{uw}_{io}}{\partial \tau} + \overline{w^2_{io}}\frac{\partial U_{io}}{\partial z_{io}} - \frac{u_*}{U_m}\overline{u\theta}_{io} + \frac{u_*}{U_m}\left(\frac{\partial \overline{uw^2}_{io}}{\partial z_{io}} + \left(\overline{w\frac{\partial p}{\partial x}}\right)_{io} + \left(\overline{u\frac{\partial p}{\partial z}}\right)_{io}\right) = 0, \tag{2.35}$$

$$\begin{aligned} &\frac{u_*^4 w_e}{w_*^5}\frac{V_g}{U_m}\frac{\partial \overline{vw}_{io}}{\partial \tau} + \overline{w^2_{io}}\frac{V_g}{U_m}\frac{\partial V_{io}}{\partial z_{io}} - \frac{u_*}{U_m}\overline{v\theta}_{io} \\ &\quad + \frac{u_*^2}{w_*^2}\frac{w_e}{w_*}\frac{V_g}{U_m}\left(\frac{\partial \overline{vw^2}_{io}}{\partial z_{io}} + \left(\overline{w\frac{\partial p}{\partial y}}\right)_{io} + \left(\overline{v\frac{\partial p}{\partial z}}\right)_{io}\right) = 0. \end{aligned} \tag{2.36}$$

The scaling of the $\overline{u\partial p/\partial z}$ can be obtained using the MMO scaling of the u–$\partial p/\partial z$ cospectrum. The results (Tong & Ding 2019, (2.16) and § 3.5) show from first principles that the spectra of u and $\partial p/\partial z$ in the convective range ($1/z_i < k < -1/L$) have scaling exponents of $-5/3$ and $-1/3$, respectively, the latter is caused by buoyancy fluctuations, where k is the horizontal wavenumber. Their cospectrum therefore has a scaling exponent no less than -1, i.e. the cospectrum cannot be steeper that k^{-1}, because u and $\partial p/\partial z$ may be less correlated at scales larger than $-L$ as it is an off-diagonal component of the velocity-pressure gradient tensor. Thus $\overline{u\partial p/\partial z}$ at $z \sim -L$ is dominated by the scales near $-L$, and therefore u_*^3/L is its proper scale. The spectral scaling exponents of w and $\partial p/\partial x$ are $1/3$ and $-1/3$, respectively,

the latter has the same scaling as $\partial p/\partial z$. Therefore $\overline{w\partial p/\partial x}$ is also dominated by the scales near $-L$ and scales as u_*^3/L. However, this term is smaller than $\overline{u\partial p/\partial z}$ because w is smaller than u at $z\sim -L$. The scaling of the velocity-pressure gradient terms is consistent with the role of these terms (partly) as the destruction rate of the shear stress. The transport term $\partial\overline{uw^2}_{io}/\partial z_{io}$ is small above the convection-induced stress layer (Businger 1973; Sykes, Henn & Lewellen 1993; Grachev, W. & Zilitinkevich 1997; Zilitinkevich *et al.* 2006; Tong & Ding 2019). The different scaling of $\overline{u\partial p/\partial z}$ in the outer and inner-outer layers also contributes to the singular nature of the problem.

There are two small parameters u_*/U_m and $(u_*^2/w_*^2)(w_e/w_*)(V_g/U_m)$ in (2.35) and (2.36), which are a result of the inner-outer scales (given in 2.32) and the terms in the budget equations. Thus, in general, we can write the inner-outer expansions of U and V as

$$U_{io}(z_{io}) = U_{io,1}(z_{io}) + \frac{u_*}{U_m}U_{io,2a}(z_{io}) + \frac{u_*^2}{w_*^2}\frac{w_e}{w_*}\frac{V_g}{U_m}U_{io,2b}(z_{io}), \tag{2.37}$$

$$\frac{V_g}{U_m}V_{io}(z_{io}) = \frac{V_g}{U_m}V_{io,1}(z_{io}) + \frac{u_*}{U_m}V_{io,2a}(z_{io}) + \frac{u_*^2}{w_*^2}\frac{w_e}{w_*}\frac{V_g}{U_m}V_{io,2b}(z_{io}), \tag{2.38}$$

thus,

$$V_{io}(z_{io}) = V_{io,1}(z_{io}) + \frac{u_*}{V_g}V_{io,2a}(z_{io}) + \frac{u_*^2}{w_*^2}\frac{w_e}{w_*}V_{io,2b}(z_{io}). \tag{2.39}$$

The velocity gradients are,

$$\frac{\partial U_{io}}{\partial z_{io}} = \frac{\partial U_{io,1}}{\partial z_{io}} + \frac{u_*}{U_m}\frac{\partial U_{io,2a}}{\partial z_{io}} + \frac{u_*^2}{w_*^2}\frac{w_e}{w_*}\frac{V_g}{U_m}\frac{\partial U_{io,2b}}{\partial z_{io}}, \tag{2.40}$$

$$\frac{\partial V_{io}}{\partial z_{io}} = \frac{\partial V_{io,1}}{\partial z_{io}} + \frac{u_*}{V_g}\frac{\partial V_{io,2a}}{\partial z_{io}} + \frac{u_*^2}{w_*^2}\frac{w_e}{w_*}\frac{\partial V_{io,2b}}{\partial z_{io}}. \tag{2.41}$$

In general, there are two inner-outer expansions, one to be matched with the outer expansion and other one to be matched with the inner-inner expansion. However, the expansions in (2.37)–(2.41) (up to the second order) can be matched with both the outer expansion and the inner expansion because it is the leading-order expansion for the velocity derivative.

Inserting $\partial U_{io}/\partial z_{io}$ and $\partial V_{io}/\partial z_{io}$ into (2.35) and (2.36), the only leading-order terms are the mean-shear production terms. Thus,

$$\frac{\partial U_{io,1}}{\partial z_{io}} = 0, \quad \frac{\partial V_{io,1}}{\partial z_{io}} = 0. \tag{2.42a,b}$$

By matching with leading-order term of the outer solution (2.18) and (2.19) (formal matching is given in (2.54)), we have

$$U_{io,1} = 1, \quad V_{io,1} = 0. \tag{2.43a,b}$$

Thus, from the inner-outer expansions (2.37) and (2.39), the inner-outer solution is,

$$U = U_m U_{io} = U_m + u_* U_{io,2a} + \frac{u_*^2}{w_*^2}\frac{w_e}{w_*}V_g U_{io,2b}, \tag{2.44}$$

$$V = V_g V_{io} = u_* V_{io,2a} + \frac{u_*^2}{w_*^2}\frac{w_e}{w_*} V_g V_{io,2b}. \tag{2.45}$$

From the inner-outer solution (2.44), we have,

$$U - U_m = u_* U_{io,2a} + \frac{u_*^2}{w_*^2}\frac{w_e}{w_*} V_g U_{io,2b}. \tag{2.46}$$

Inserting $\partial U_{io}/\partial z_{io}$ (2.40) into (2.35) leads to $\partial U_{io,2b}/\partial z_{io} = 0$, since at the second order, equation (2.35) does not contain the parameter $(u_*^2/w_*^2)(w_e/w_*)(V_g/U_m)$ (§ 2.3 further shows that $U_{io,2b} = 0$). Equation (2.46) is another new velocity-defect law, the surface-layer velocity-defect law, in the convective atmospheric boundary layer. Thus the z/L dependence of U is in the form of a velocity-defect law, not the law of the wall. The term 'surface layer' here is used to indicate that the range of heights within which this velocity-defect law is valid is inside the surface layer, not that the defect law is valid in the entire surface layer. Equation (2.43) shows that U_m is also the upper boundary condition for the leading-order velocity in the inner-outer layer (due to the asymptotically small velocity defect in the outer layer), indicating that the mean velocity in this layer is coupled to the mixed layer rather than to the surface. Again, previous works (e.g. Zilitinkevich & Deardorff 1974; Garratt *et al.* 1982) used $U - U_g$ as the defect, which does not reflect the velocity defect in the surface layer.

We note that the surface-layer velocity-defect law cannot be obtained using MOST, as the velocity scale U_m is not a parameter in the Monin–Obukhov similarity. Since MOST only involve the surface-layer parameters, it can only provide the Monin–Obukhov similarity functions. The surface-layer velocity-defect law, on the other hand, also needs to include U_m.

The inner-outer layer also limits the extent of the outer layer. In the neutral ABL the outer layer extends down to heights $z \gg h_0$. In the CBL, on the other hand, it only extends down to heights of order $-L$ due to the small velocity defect in the outer layer. Note that the inner-outer solution (2.43) is not valid in the roughness layer, indicating that there is still another singular (inner) layer.

Similarly, inserting $\partial V_{io}/\partial z_{io}$ (2.41) into (2.36) leads to $\partial V_{io,2a}/\partial z_{io} = 0$, since at the second order, equation (2.36) does not contain the parameter u_*/V_g (§ 2.3 shows that $V_{io,2a} = 0$). We evaluate the magnitude of V using typical values of u_*, w_*, w_e and V_g,

$$V \sim \frac{u_*^2}{w_*^2}\frac{w_e}{w_*} V_g \sim \frac{0.3^2}{2^2}\frac{0.03}{2} \times 1 \sim 4 \times 10^{-4}\ \mathrm{m\ s^{-1}}, \tag{2.47}$$

indicating that the change in the direction of the mean velocity direction in this layer is also negligible.

The equation for the second-order term $U_{io,2a}$ is,

$$\frac{u_*^2}{w_*^2}\frac{\partial \overline{uw}_{io,1}}{\partial \tau} + \overline{w_{io,1}^2}\frac{\partial U_{io,2a}}{\partial z_{io}} - \overline{u\theta}_{io,1} + \frac{\partial \overline{uw^2}_{io,1}}{\partial z_{io}} + \left(\overline{w\frac{\partial p}{\partial x}}\right)_{io} + \left(\overline{u\frac{\partial p}{\partial z}}\right)_{io} = 0. \tag{2.48}$$

Equation (2.48) contains a small parameter u_*^2/w_*^2 in the time derivative term, which becomes order one in (2.22) (the outer layer). In addition, the scaling of $\overline{w^2}$ and $\overline{u\partial p/\partial z}$ changes when z increases from $z < -L$ to $z \gg -L$, as discussed in section (2.1). Therefore (2.22) and (2.48) form a singular perturbation problem. The leading-order expansions $U_{o,2a}$ and $U_{io,2a}$ can be obtained by the method of matched asymptotic expansions.

From the mean momentum equation for V, we can write the inner-outer expansion of $\partial\overline{vw}/\partial z$ as

$$\frac{\partial\overline{vw}_{io}}{\partial z_{io}} = \frac{U_g - U_m}{(u_*^2 w_e)/(f^2 z_i^2)} - \frac{u_* U_{io,2a}}{(u_*^2 w_e)/(f^2 z_i^2)}, \\ = 1 - \frac{f^2 z_i^2}{u_* w_e} U_{io,2a}, \tag{2.49}$$

where,

$$\frac{f^2 z_i^2}{u_* w_e} \sim \frac{0.01}{0.3 \times 0.03} \sim 1. \tag{2.50}$$

Thus there are also significant variations of the gradient of $\overline{vw}_{io}$ in the inner-outer layer. From the mean momentum equation for U, we can write the inner-outer expansion of $\partial\overline{uw}/\partial z$,

$$\frac{\partial\overline{uw}_{io}}{\partial z_{io}} = -\frac{fL}{u_*^2}(V - V_g) = -\frac{L}{z_i} + \frac{L}{z_i}\frac{u_*^2}{w_*^2}\frac{w_e}{w_*} V_{io,2b} \ll 1. \tag{2.51}$$

Thus, the variations of the gradient of $\overline{uw}_{io}$ in the inner-outer layer are of higher order, (i.e. the stress is approximately constant). Although the variations of the $\overline{vw}_{io}$ gradient are of order one, $\overline{vw}$ itself is of higher order compared to $\overline{uw}$. Thus, the behaviour of the inner-outer layer at the leading order is not affected by Earth's rotation.

2.3. *Matching between the outer and the inner-outer expansion*

The mean velocity in terms of the outer expansion (up to the second order) is

$$U = U_m U_o = U_m \left(1 + \frac{u_*}{w_*}\frac{u_*}{U_m} U_{o,2a} + \frac{w_e}{w_*}\frac{V_g}{U_m} U_{o,2b}\right). \tag{2.52}$$

In terms of the inner-outer expansion, it is

$$U = U_m U_{io} = U_m \left(1 + \frac{u_*}{U_m} U_{io,2a} + \frac{u_*^2}{w_*^2}\frac{w_e}{w_*}\frac{V_g}{U_m} U_{io,2b}\right). \tag{2.53}$$

Matching the two expansions we have

$$U_m \left(1 + \frac{u_*}{w_*}\frac{u_*}{U_m} U_{o,2a} + \frac{w_e}{w_*}\frac{V_g}{U_m} U_{o,2b}\right) = U_m \left(1 + \frac{u_*}{U_m} U_{io,2a} + \frac{u_*^2}{w_*^2}\frac{w_e}{w_*}\frac{V_g}{U_m} U_{io,2b}\right). \tag{2.54}$$

For the parameter $(u_*/w_*)(u_*/U_m)$, we have

$$\frac{u_*}{w_*} u_* U_{o,2a}\left(\frac{z}{z_i}\right) = u_* U_{io,2a}\left(-\frac{z}{L}\right). \tag{2.55}$$

Thus,

$$\frac{u_*}{w_*}\left(\frac{z}{L}\frac{L}{z_i}\right)^{\alpha} = \left(-\frac{z}{L}\right)^{\alpha}, \quad \alpha = -\frac{1}{3}, \tag{2.56}$$

because L/z_i has to cancel on the left-hand side (note that $-L/z_i \sim (u_*/w_*)^3$). This leads to

$$U_{o,2a} = A_u \left(\frac{z}{z_i}\right)^{-1/3}, \quad U_{io,2a} = A_u \left(-\frac{z}{L}\right)^{-1/3}. \tag{2.57a,b}$$

For the parameter $(w_e/w_*)(V_g/U_m)$, we have

$$\frac{w_e}{w_*} V_g U_{o,2b}\left(\frac{z}{z_i}\right) = \frac{u_*^2}{w_*^2}\frac{w_e}{w_*} V_g U_{io,2b}\left(-\frac{z}{L}\right), \tag{2.58}$$

$$\frac{u_*^2}{w_*^2}\left(-\frac{z_i}{L}\frac{z}{z_i}\right)^{\beta} = \left(\frac{z}{z_i}\right)^{\beta}, \quad \beta = \frac{2}{3}, \tag{2.59}$$

leading to

$$U_{o,2b} = B_u \left(\frac{z}{z_i}\right)^{2/3}, \quad U_{io,2b} = B_u \left(-\frac{z}{L}\right)^{2/3}. \tag{2.60a,b}$$

However, since $\partial U_{o,2b}/\partial z_o = 0$, we have $B_u = 0$; thus $U_{o,2b} = U_{io,2b} = 0$. From (2.57) and (2.60) we can write

$$U = U_m + u_* A_u \left(-\frac{z}{L}\right)^{-1/3}. \tag{2.61}$$

This is the velocity profile in the local-free-convection scaling layer. Monin & Obukhov (1954) predicted the $(-z/L)^{-1/3}$ scaling, but did not predict it as a velocity defect.

Similarly, for the V component of the mean velocity, matching results in

$$V_{o,2a} = A_v \left(\frac{z}{z_i}\right)^{-1/3}, \quad V_{io,2a} = A_v \left(-\frac{z}{L}\right)^{-1/3}, \tag{2.62a,b}$$

and

$$V_{o,2b} = B_v \left(\frac{z}{z_i}\right)^{2/3}, \quad V_{io,2b} = B_v \left(-\frac{z}{L}\right)^{2/3}. \tag{2.63a,b}$$

Since $\partial V_{o,2a}/\partial z_o = 0$, we have $A_v = 0$; thus $V_{o,2a} = V_{io,2a} = 0$. Thus we can write

$$V = B_v V_g \frac{u_*^2}{w_*^2}\frac{w_e}{w_*}\left(-\frac{z}{L}\right)^{2/3}. \tag{2.64}$$

2.4. *The inner-inner expansion*

The inner-inner layer has a length scale of h_0 and a velocity scale of u_* (Tong & Ding 2018). We use U_m, V_g, u_*^2, h_0 and Q to define the dimensionless inner-inner variables as follows:

$$\left.\begin{aligned} U(z) = U_m U_{ii}\left(\frac{z}{h_0}\right), \quad V(z) = V_g V_{ii}\left(\frac{z}{h_0}\right), \quad \overline{uw} = u_*^2 \overline{uw}_{ii}, \\ \overline{vw} = fU_g(-L)\overline{vw}_{ii}, \quad z = h_0 z_{ii}, \quad \overline{u\theta} = Q\overline{u\theta}_{ii}, \quad \overline{w^2} = u_*^2 \overline{w^2_{ii}}. \end{aligned}\right\} \tag{2.65}$$

The scale for $\overline{vw}$ is obtained by integrating the leading-order mean momentum equation $\partial \overline{vw}/\partial z = fU_g$ from h_0 to $-L$, with the upper limit determined by the fact

that the vertical derivative of the lateral stress matches that due to the entrainment. The shear-stress budget equations are as follows:

$$\frac{\partial \overline{uw}_{ii}}{\partial \tau}\frac{u_*^2 w_*}{z_i}+u_*^2\overline{w_{ii}^2}\frac{U_m}{h_0}\frac{\partial U_{ii}}{\partial z_{ii}}-\frac{g}{T}Q\overline{u\theta}_{ii}+\frac{u_*^3}{h_0}\left(\frac{\partial \overline{uw^2}_{ii}}{\partial z_{ii}}+\left(\overline{w\frac{\partial p}{\partial x}}\right)_{ii}+\left(\overline{u\frac{\partial p}{\partial z}}\right)_{ii}\right)=0, \tag{2.66}$$

$$\frac{\partial \overline{vw}_{ii}}{\partial \tau}fU_g(-L)\frac{w_*}{z_i}+u_*^2\overline{w_{ii}^2}\frac{V_g}{h_0}\frac{\partial V_{ii}}{\partial z_{ii}}-\frac{g}{T}Q\overline{v\theta}_{ii}$$
$$+\frac{u_*}{h_0}fU_g(-L)\left(\frac{\partial \overline{vw^2}_{ii}}{\partial z_{ii}}+\left(\overline{w\frac{\partial p}{\partial y}}\right)_{ii}+\left(\overline{v\frac{\partial p}{\partial z}}\right)_{ii}\right)=0. \tag{2.67}$$

Dividing (2.66) and (2.67) by $u_*^2U_m/h_0$ results in the non-dimensional shear-stress budget equations in the inner-inner layer,

$$\frac{h_0}{z_i}\frac{w_*}{U_m}\frac{\partial \overline{uw}_{ii}}{\partial \tau}+\overline{w_{ii}^2}\frac{\partial U_{ii}}{\partial z_{ii}}-\frac{(g/T)Qh_0}{u_*^2U_m}\overline{u\theta}_{ii}+\frac{u_*}{U_m}\left(\frac{\partial \overline{uw^2}_{ii}}{\partial z_{ii}}+\left(\overline{w\frac{\partial p}{\partial x}}\right)_{ii}+\left(\overline{u\frac{\partial p}{\partial z}}\right)_{ii}\right)=0, \tag{2.68}$$

$$\frac{h_0}{z_i}\frac{f(-L)w_*}{u_*^2}\frac{U_g}{U_m}\frac{\partial \overline{vw}_{ii}}{\partial \tau}+\overline{w_{ii}^2}\frac{V_g}{U_m}\frac{\partial V_{ii}}{\partial z_{ii}}-\frac{(g/T)Qh_0}{u_*^2U_m}\overline{v\theta}_{ii}$$
$$+\frac{f(-L)}{u_*}\frac{U_g}{U_m}\left(\frac{\partial \overline{vw^2}_{ii}}{\partial z_{ii}}+\left(\overline{w\frac{\partial p}{\partial y}}\right)_{ii}+\left(\overline{v\frac{\partial p}{\partial z}}\right)_{ii}\right)=0. \tag{2.69}$$

Similar to the inner-outer layer, the scaling of the $\overline{u\partial p/\partial z}$ can be obtained using the MMO scaling of the u–$\partial p/\partial z$ cospectrum. Tong & Ding (2019) have shown that the spectrum of u in the dynamic range have scaling exponents of -1. Near $kz=1$, $\partial p/\partial z$ is balanced by the nonlinear term (N3) in equation (3.19) in Tong & Ding (2019), which has a spectral scaling exponent of 3. Therefore the $u-\partial p/\partial z$ cospectrum has a scaling exponent no less than 1. Thus $\overline{u\partial p/\partial z}$ is dominated by the scales near z, and u_*^3/z is its proper scale. Similarly, the spectral scaling of w and $\partial p/\partial x$ are both 1. Thus, $\overline{w\partial p/\partial x}$ is also determined by the scales near z, thus having a scale of u_*^3/z. For $z\to h_0$, we expect that u_*^2/h_0 is the proper scale for these quantities. Again, the transport term is small.

Similar to (2.35) and (2.36) in the inner-outer layer, there are also two small (independent) parameters u_*/U_m and $(f(-L)/u_*)(U_g/U_m)$ in the (2.68) and (2.69). Thus, we can write the inner-inner expansions as

$$U_{ii}(z_{ii})=U_{ii,1}(z_{ii})+\frac{u_*}{U_m}U_{ii,2}(z_{ii}), \tag{2.70}$$

$$\frac{V_g}{U_m}V_{ii}(z_{ii})=\frac{V_g}{U_m}V_{ii,1}(z_{ii})+\frac{f(-L)}{u_*}\frac{U_g}{U_m}V_{ii,2}(z_{ii}), \tag{2.71}$$

thus,

$$V_{ii}(z_{ii})=V_{ii,1}(z_{ii})+\frac{f(-L)}{u_*}\frac{U_g}{V_g}V_{ii,2}(z_{ii}). \tag{2.72}$$

The velocity gradients are

$$\frac{\partial U_{ii}}{\partial z_{ii}}=\frac{\partial U_{ii,1}}{\partial z_{ii}}+\frac{u_*}{U_m}\frac{\partial U_{ii,2}}{\partial z_{ii}}, \tag{2.73}$$

$$\frac{\partial V_{ii}}{\partial z_{ii}} = \frac{\partial V_{ii,1}}{\partial z_{ii}} + \frac{f(-L)}{u_*}\frac{U_g}{V_g}\frac{\partial V_{ii,2}}{\partial z_{ii}}. \tag{2.74}$$

Inserting $\partial U_{ii}/\partial z_{ii}$ and $\partial V_{ii}/\partial z_{ii}$ into (2.68) and (2.69), the only leading-order terms are the mean-shear production terms. Thus,

$$\frac{\partial U_{ii,1}}{\partial z_{ii}} = 0, \quad \frac{\partial V_{ii,1}}{\partial z_{ii}} = 0, \tag{2.75a,b}$$

and

$$U_{ii,1} = 0, \quad V_{ii,1} = 0, \tag{2.76a,b}$$

since $U_{ii,1}$ and $V_{ii,1}$ must equal zero at some z value, which can be defined as h_0. Thus, we can write the inner-inner solution as,

$$U = U_m U_{ii} = u_* U_{ii,2}(z_{ii}), \tag{2.77}$$

$$V = V_g V_{ii} = \frac{f(-L)}{u_*} U_g V_{ii,2}(z_{ii}). \tag{2.78}$$

For a strongly convective boundary layer, e.g. $-L = 20$ m, $u_* = 0.3$ m s^{-1}, $U_g = 5$ m s^{-1}, the lateral velocity is of order $f(-L)U_g/u_* = 0.03$ m s^{-1}, which is relatively small.

The mean momentum equation for V is

$$\frac{\partial \overline{vw}_{ii}}{\partial z_{ii}} = \frac{h_0}{-L} - \frac{h_0}{-L}\frac{u_*}{U_g} U_{ii,2} + \frac{\mathrm{d}\tau_{ryii}}{\mathrm{d}z_{ii}}. \tag{2.79}$$

The mean momentum equation for U is

$$\frac{\partial \overline{uw}_{ii}}{\partial z_{ii}} = \frac{h_0}{z_i} - \frac{h_0}{z_i}\frac{V}{V_g} + \frac{\mathrm{d}\tau_{rxii}}{\mathrm{d}z_{ii}} = \frac{h_0}{z_i} - \frac{h_0}{z_i}\frac{f(-L)}{u_*}\frac{U_g}{V_g} V_{ii,2} + \frac{\mathrm{d}\tau_{rxii}}{\mathrm{d}z_{ii}}. \tag{2.80}$$

Integrating these equations from h_0 to z_{ii} and keeping the leading-order results in

$$\overline{vw}_{ii,1} = 1 - \tau_{ryii,1}, \tag{2.81}$$

$$\overline{uw}_{ii,1} = 1 - \tau_{rxii,1}. \tag{2.82}$$

Again, since $\overline{vw}$ is much smaller than $\overline{uw}$, the behaviours of the inner-inner layer at the leading order is not affected by Earth's rotation at the leading order.

The equation for the second term $U_{ii,2}$ is,

$$\frac{h_0}{z_i}\frac{w_*}{u_*}\frac{\partial \overline{uw}_{ii}}{\partial \tau} + \overline{w_{ii}^2}\frac{\partial U_{ii,2}}{\partial z_{ii}} - \frac{(g/T)Qh_0}{u_*^3}\overline{u\theta}_{ii} + \left(\frac{\partial \overline{uw^2}_{ii}}{\partial z_{ii}} + \left(\overline{w\frac{\partial p}{\partial x}}\right)_{ii} + \left(\overline{u\frac{\partial p}{\partial z}}\right)_{ii}\right) = 0. \tag{2.83}$$

Equation (2.83) contains a small parameter $(g/T)Qh_0/u_*^3$ in the $\overline{u\theta}_{ii}$ term, which becomes order one in (2.48) (the inner-outer layer), and is a correction due to buoyancy production as $z \to -L$. The roughness contribution (as part of the pressure terms) in (2.48) is of higher order, which becomes order one in (2.83). Thus (2.48) and (2.83) also form a singular perturbation problem. The leading-order expansions $U_{io,2a}$ and $U_{ii,2}$ can be obtained by the method of matched asymptotic expansions.

2.5. *Matching between the inner-outer and the inner-inner expansion*

The mean velocity in terms of the inner-outer expansion is

$$U = U_m U_{io} = U_m + u_* U_{io,2a}(z_{io}). \tag{2.84}$$

In terms of the inner-inner expansion, it is

$$U = U_m U_{ii} = u_* U_{ii,2}(z_{ii}). \tag{2.85}$$

Matching the two expansions results in

$$U_{ii,2}\left(-z_{io}\frac{L}{h_0}\right) = \frac{U_m}{u_*} + U_{io,2a}(z_{io}). \tag{2.86}$$

This equation shows that U_m/u_* is a function of $-L/h_0$. Differentiating equation (2.86) with respect to z_{io} results in

$$\frac{\partial U_{ii,2}}{\partial z_{io}} = -\frac{\mathrm{d}U_{ii,2}}{\mathrm{d}z_{ii}}\frac{L}{h_0} = \frac{\mathrm{d}U_{io,2a}}{\mathrm{d}z_{io}}. \tag{2.87}$$

Thus

$$\frac{\mathrm{d}U_{ii,2}}{\mathrm{d}z_{ii}} z_{ii} = \frac{\mathrm{d}U_{io,2a}}{\mathrm{d}z_{io}} z_{io} = \frac{1}{\kappa}, \tag{2.88}$$

where κ does not depend on either z_{ii} or z_{io}, and therefore does not depend on $-L/h_0$. Differentiating equation (2.86) with respect to $-L/h_0$ results in

$$-\frac{\partial U_{ii,2}}{\partial L/h_0} = \frac{\mathrm{d}U_{ii,2}}{\mathrm{d}z_{ii}} z_{io} = -\frac{\mathrm{d}U_{ii,2}}{\mathrm{d}z_{ii}} z_{ii}\frac{h_0}{L} = -\frac{\mathrm{d}U_m/u_*}{\mathrm{d}L/h_0}. \tag{2.89}$$

The last term in (2.89) does not depend on z_{ii}. From (2.89) we obtain

$$U_{ii,2} = \frac{\mathrm{d}U_m/u_*}{\mathrm{d}L/h_0}\frac{L}{h_0}\ln z_{ii} = \frac{1}{\kappa}\ln z_{ii} = \frac{1}{\kappa}\ln\frac{z}{h_0}. \tag{2.90}$$

Note that this expression is valid only in the matching layer. This h_0 is defined by extrapolating the profile to $U_{ii,2} = 0$. From (2.88) we obtain

$$U_{io,2a} = \frac{\mathrm{d}U_m/u_*}{\mathrm{d}L/h_0}\frac{L}{h_0}\ln z_{io} + C = \frac{1}{\kappa}\ln z_{io} + C = \frac{1}{\kappa}\ln\left(-\frac{z}{L}\right) + C. \tag{2.91}$$

Hence,

$$U = U_m + u_*\left(\frac{1}{\kappa}\ln\left(-\frac{z}{L}\right) + C\right). \tag{2.92}$$

Equation (2.90) provides a physical interpretation of the (inverse of) the von Kármán constant

$$\frac{1}{\kappa} = \frac{\mathrm{d}U_m/u_*}{\mathrm{d}\ln(-L/h_0)}. \tag{2.93}$$

It is the rate of change of the friction velocity ratio U_m/u_* with respect to the logarithm of the ratio of the height of the shear-production-dominant layer to the roughness height. In a neutral boundary layer, it becomes

$$\frac{1}{\kappa} = \frac{\mathrm{d}U_m/u_*}{\mathrm{d}\ln z_i/h_0}, \tag{2.94}$$

which also has a clear physical interpretation. Equations (2.90) and (2.91) are the log law and the surface-layer velocity-defect law in the matching layer. Combining the two equations results in

$$\frac{U_m}{u_*} = \frac{1}{\kappa} \ln\left(-\frac{L}{h_0}\right) - C. \tag{2.95}$$

Differentiating this equation with respect to $-L/h_0$ and considering (2.93), we find that C also does not depend on $-L/h_0$, and therefore is a constant. Equation (2.95) is the logarithmic friction law for the convective atmospheric boundary layer, which we term the convective logarithmic friction law. Thus, for the same U_m, the surface stress increases with the surface temperature flux. Compared with the logarithmic friction law for neutral boundary layers, the Obukhov length replaces the boundary layer (inversion) height, because the convective eddies result in an asymptotically small mean velocity gradient in the mixed layer, pushing U_m down to the height $-L$.

The discovery of the convective logarithmic friction law allows us to make several comments on the previous geostrophic drag laws (or resistance laws) (Lettau 1959; Kazanski & Monin 1960; Csanady 1967; Blackadar & Tennekes 1968; Brown 1973; Zilitinkevich & Deardorff 1974; Zilitinkevich 1975; Zilitinkevich *et al.* 1992). First, the convective logarithmic friction law is derived analytically from first principles whereas the geostrophic drag law was largely based on phenomenology. Second, the convective logarithmic friction law is derived from the law of the wall and the surface-layer velocity-defect law and is an exact leading-order result relating u_* to the velocity scale U_m, not an extrapolation of the log law. No approximate velocity is used. By contrast, some previous drag laws (e.g. Zilitinkevich *et al.* 1992) match the geostrophic wind with an approximate velocity beyond the log layer (at a height $z \sim z_i$), and therefore are inherently approximate and empirical. Third, as mentioned above, the convective logarithmic friction law is derived using the velocity defect $U - U_m$ which scales with u_* in the surface layer, whereas some other previous drag laws (e.g. Zilitinkevich & Deardorff 1974; Zilitinkevich 1975) used the velocity defect $U - U_g$, part of which $(U_m - U_g)$ does not scale with u_* (2.26). Since u_* is completely determined by U_m and L/h_0, $U_m - U_g$ does not play a role in determining the friction, and therefore should not be an inherent part of the drag law. Garratt *et al.* (1982) proposed a geostrophic drag law assuming that the mean velocity at the top of the surface layer equals that in the mixed layer. However, it uses the empirical stability function ψ_m, which may be inaccurate for large values of $-z/L$, whereas the convective logarithmic friction law does not involve any empirical functions.

2.6. *Overall mean velocity profile*

The different functional forms of mean velocity in the three layers discussed in the preceding subsections form an overall mean velocity profile. A schematic including the relationships among the different layers and scaling ranges is shown in figure 1. In a neutral ABL, the inner layer, where the law of the wall is valid, covers the entire surface layer. The outer layer, where the velocity-defect law holds, extends into the surface layer, down to a height $z \gg h_0$. By contrast, in a CBL, the inner-inner layer, where the law of the wall (for rough wall) is valid, only extends to a height $z < -L$. The inner-outer layer covers the rest of the surface layer ($h_0 \ll z \ll z_i$), and follows the surface-layer velocity-defect law, with the velocity scale u_*. The outer layer extends into the surface layer, but only down to $z \gg -L$, and follows the mixed-layer velocity-defect law, with the velocity scale u_*^2/w_*. There are two overlapping layers in which

the mean velocity profile conforms to the log law and the local-free-convection scaling, respectively.

The surface-layer velocity-defect law provides an important interpretation of the velocity profile given in Monin & Obukhov (1954),

$$U(z) = \frac{u_*}{\kappa}\left[f\left(\frac{z}{L}\right) - f\left(\frac{h_0}{L}\right)\right], \tag{2.96}$$

where

$$f\left(\frac{z}{L}\right) = \int \frac{\phi_m(z/L)}{z/L} d\left(\frac{z}{L}\right). \tag{2.97}$$

For $h_0/L \ll 1$, $f(h_0/L) \approx \ln(L/h_0)$ since $\phi_m(0) = 1$. Thus,

$$U(z) \approx \frac{u_*}{\kappa}\left[f\left(\frac{z}{L}\right) + \ln\left(\frac{L}{h_0}\right)\right]. \tag{2.98}$$

Using the convective logarithmic friction law (2.95), we can write

$$U(z) \approx \frac{u_*}{\kappa}\left[f\left(\frac{z}{L}\right) + \frac{U_m\kappa}{u_*} + \kappa C\right], \tag{2.99}$$

and

$$U - U_m \approx \frac{u_*}{\kappa}\left[f\left(\frac{z}{L}\right) + \kappa C\right]. \tag{2.100}$$

Thus $f(z/L)$ is essentially part of the velocity defect. However, this relationship only becomes clear with the derivation of the surface-layer defect-law.

The surface-layer velocity-defect law also provides an understanding of another form of the velocity profile (Panofsky & Dutton 1984),

$$\frac{U}{u_*} = \frac{1}{\kappa}\left[\ln\frac{z}{h_0} - \psi_m\left(\frac{z}{L}\right)\right], \tag{2.101}$$

where

$$\psi_m\left(\frac{z}{L}\right) = \int_0^{z/L} [1 - \phi_m(\zeta)]\frac{\mathrm{d}\zeta}{\zeta}. \tag{2.102}$$

We note that (2.102) is only valid for $z/h_0 \gg 1$, i.e. in the matching (log) layer and above, because it is obtained using the non-dimensional mean shear $\phi_m(z/L)$, which has the same region of validity. Furthermore, although (2.101) might give the impression of a modified law of the wall (with an added dependence on $-z/L$), in which a wall velocity scale (u_*) and a wall length scale (h_0) are involved, it is not one. This can be seen from the surface-layer velocity-defect law (2.46), which shows that the dependence of U on $-z/L$ comes entirely in the form of the velocity defect and does not depend on h_0 (part of ψ_m cancels the logarithmic term in (2.101)).

To further examine (2.101), we derive it by inserting U_m (2.95) into the surface-layer defect-law (2.46),

$$\begin{aligned} U &= \frac{u_*}{\kappa}\ln\left(-\frac{L}{h_0}\right) - u_*C + u_*U_{io,2a} \\ &= \frac{u_*}{\kappa}\left[\ln\frac{z}{h_0} + \ln\left(-\frac{L}{z}\right)\right] - u_*C + u_*U_{io,2a} \\ &= \frac{u_*}{\kappa}\ln\frac{z}{h_0} - \frac{u_*}{\kappa}\ln\left(-\frac{z}{L}\right) - u_*C + u_*U_{io,2a}. \end{aligned} \tag{2.103}$$

It can be seen that $\psi_m(z/L)$ contains the velocity defect which, however, also only becomes clear with the derivation of (2.46). Since (2.101) was obtained without the knowledge of the surface-layer velocity-defect law, it could only be obtained empirically.

The defect law (2.46) also shows that for $z \sim -L$, the mean velocity U is of order U_m because $U_m - U \sim u_* \ll U_m$. This behaviour, however, cannot be inferred from (2.96) and (2.101) as they do not contain U_m. Thus, while numerically the empirical velocity profile (2.101) has the correct behaviour and is useful for practical applications, its origin and interpretation only become clear with the discovery of the surface-layer velocity-defect law. From a practical point of view, it may be more accurate to use the surface-layer velocity-defect law rather than (2.101) for $z/L \gtrsim 1$, as it is the difference of two large terms (the term $\ln(z/h_0)$ is actually cancelled).

The surface-layer velocity-defect law indicates that buoyancy effects reduce the extent of the law of the wall. In a neutral boundary layer, the law of the wall is valid in the entire surface layer. By contrast, in a convective boundary layer, it is only valid up to $z < -L$, i.e. it ceases to be valid as z approaches $-L$. Thus buoyancy disrupts the law of the wall rather than modifying it. A key factor for the law of the wall is the no-slip boundary condition (at $z = h_0$). For $z \geqslant -L$ the larger vertical velocity variance due to buoyancy production reduces the outer-layer velocity defect, imposing U_m as the (upper) boundary condition on the leading-order inner-outer layer velocity, thereby disrupting the law of the wall and resulting in the surface-layer velocity-defect law. This defect law suggests that $-L$ can also be interpreted as the height at which the mean velocity ceases to be coupled to the surface velocity, and instead becomes coupled to the mixed-layer velocity scale U_m.

3. Comparisons with LES

In this section we compare the velocity-defect laws and the logarithmic friction law with the mean velocity profiles obtained using LES with different $-z_i/L$ values as shown in table 1. Since the scaling laws are obtained for the barotropic CBL, comparisons with field data would require information about the horizontal mean temperature gradient to ensure that baroclinic effects are negligible. We will leave such comparisons to future studies.

We used the LES formulation described in detail in Moeng (1984). It has been well documented in the literature (Moeng & Wyngaard 1988; Sullivan, McWilliams & Moeng 1994, 1996) and refined later by Otte & Wyngaard (2001). The LES code solves the spatially filtered momentum equation for Boussinesq flow and a transport equation for a filtered conserved scalar, supplemented with a transport equation for the subgrid-scale turbulent kinetic energy. The LES code uses pseudo-spectra representation in the horizontal directions and first-order finite difference in the vertical direction, the latter implemented on a staggered mesh to maintain tight velocity–pressure coupling. A third-order Runge–Kutta scheme (Spalart, Moser & Rogers 1991, Sullivan *et al.* 1996) is used for the time stepping. Assuming that the mean wind and mean stress obey the Monin–Obukhov scaling, we follow the procedure described by Moeng (1984) and compute the surface friction velocity u_* from the horizontal-mean wind speed at the first grid level. The local stress at each grid point at the surface is then computed from u_* based on the procedure described in the appendix of Moeng (1984), where the wind in the surface drag law is decomposed into mean and fluctuating components. At the lower boundary, the surface stress and flux are estimated using wall functions based on MOST (Businger

	SGS model	U_g (m s^{-1})	Q (K m s^{-1})	u_* (m s^{-1})	$-L$ (m)	z_i z_i (m)	w_* (m s^{-1})	θ_* (K)	$-z_i/L$ (1)
(1)	Kosović	15	0.20	0.74	154.0	1045	1.89	0.11	6.79
(2)	Kosović*	10	0.08	0.53	144.2	1011	1.38	0.05	7.01
(3)	Smagorinsky	15	0.20	0.71	137.2	1040	1.88	0.11	7.58
(4)	Smagorinsky	10	0.12	0.56	115.0	1092	1.62	0.07	9.50
(5)	Kosović*	10	0.18	0.59	87.2	1031	1.81	0.10	11.82
(6)	Smagorinsky*	10	0.12	0.51	84.9	1030	1.59	0.08	12.13
(7)	Kosović	10	0.20	0.56	69.5	1048	1.89	0.11	15.08
(8)	Smagorinsky	10	0.20	0.54	61.8	1055	1.89	0.11	17.07
(9)	Kosović	9	0.20	0.52	54.5	1095	1.91	0.10	20.09
(10)	Smagorinsky	9	0.20	0.51	49.8	1088	1.91	0.10	21.85
(11)	Smagorinsky*	9	0.20	0.50	47.4	1081	1.91	0.10	22.81
(12)	Smagorinsky	8	0.20	0.47	39.4	1092	1.91	0.11	27.72
(13)	Smagorinsky	8	0.24	0.48	34.5	1095	2.03	0.12	32.17
(14)	Kosović*	6	0.20	0.40	25.3	1099	1.92	0.10	43.41

TABLE 1. Large-eddy simulation parameters for 512^3 and 1024^3 (*) resolutions. All simulations are implemented with a domain size of 5120 m × 5120 m in the horizontal directions and 2048 m in the vertical direction. The grid sizes (Δ_x, Δ_y, Δ_z) for 512^3 and 1024^3 resolutions are (10 m, 10 m, 4 m) and (5 m, 5 m, 2 m), respectively.

et al. 1971). The Smagorinsky model (Smagorinsky 1963; Lilly 1967; Moeng 1984) and Kosović model (Kosović 1997) are employed to parameterize the subgrid-scale (SGS) fluxes.

The velocity scale U_m in the velocity-defect laws is given in (2.26). However, since w_e is not known in the present study (its determination is beyond the scope of this study), we determine U_m using an empirical approach involving two methods as follows. In the first method, we choose the U_m value for each U profile such that the curves collapse near the outer layer ($z/z_i \sim 0.2$), thus determining U_m for each profile up to a (common) constant. We then determine the constant by varying it until $(U_m - U)/(u_*^2/w_*)$ has an approximate $(z/z_i)^{-1/3}$ scaling in the overlapping region with the inner-outer layer. We note that the $(z/z_i)^{-1/3}$ scaling is consistent with the $(z/z_i)^{-4/3}$ scaling for the mean velocity gradient obtained using LES (not shown). In the second method, we collapse profiles in the inner-outer layer ($-z/L \sim 1$), determining another U_m value for each curve, again up to a (common) constant. We again determine the constant by varying it until $(U_m - U)/u_*$ has a $(-z/L)^{-1/3}$ scaling in the overlapping region with the outer layer. The U_m values determined using the two methods are compared in figure 2. The difference between the values for each case is typically less than 0.1 m s^{-1}, corresponding to approximately 10 % of the $(U_m - U)$ value near $-z/L \sim 1$. Therefore the two methods yield consistent results, indicating the effectiveness of the approach, and providing support to the velocity-defect laws.

The mixed-layer velocity-defect profiles obtained from LES with several $-z_i/L$ values employing the Smagorinsky model are shown in figure 3(*a*). The profiles collapse well in the mixed layer up to $z/z_i = 0.4$, supporting the mixed-layer velocity-defect law. For $z/z_i > 0.4$, the differences among the profiles are larger, perhaps due to the effects of the inversion layer.

The surface-layer velocity-defect law profiles (figure 4*a*) also collapse well near $-z/L = 1$. The overlapping region also has a $(-z/L)^{-1/3}$ scaling. While several profiles

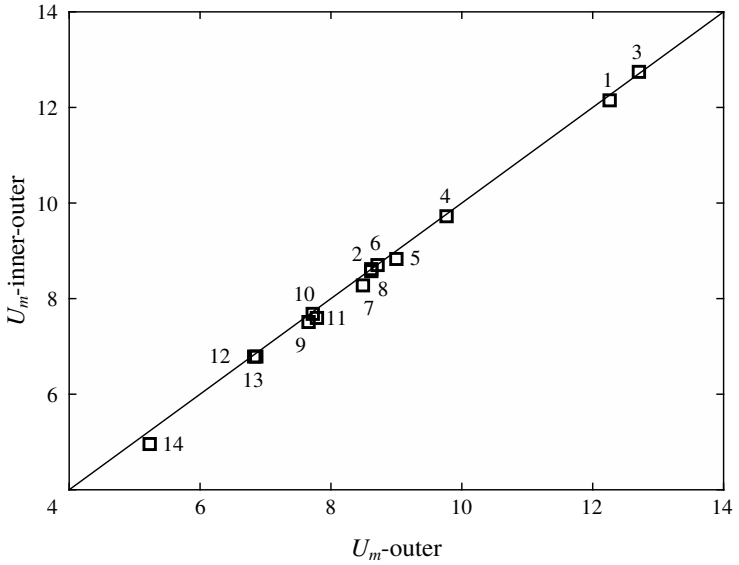

FIGURE 2. The values of the mixed-layer mean velocity scale U_m determined using two methods: collapsing profiles in the outer layer (x-axis) and collapsing profiles in the inner-outer layer (y-axis). The number next to each square denotes the LES run (table 1).

show a log region (figure 5*a*), those with larger $-z_i/L$ do not, due to the lack of LES resolution for $z \ll -L$ and the well known overshoot in the non-dimensional mean shear associated with the Smagorinsky model (Mason & Thomson 1992). Brasseur & Wei (2010) proposed a method to solve the overshoot problem through a combination of the model coefficient and resolution. However, the potential effects on the statistics of fluctuating variables are not clear at this time. Exploring these effects is beyond the scope of this work. Therefore, we do not employ this method to eliminate the overshoot.

The velocity defects obtained from LES employing the Kosović model are shown in figures 3(*b*), 4(*b*) and 5(*b*). The log law is more evident, due to the absence of the overshoot problem for this model. The collapse is better than the Smagorinsky model, providing further support for the velocity-defect laws. We note that the values of the model coefficients in the Kosović model are the same as those in Miles, Wyngaard & Otte (2004), which have not been fine-tuned to optimize the model performance, because we are interested in the scaling properties, not the accuracy of the mean velocity profiles. While the velocity-defect profiles for the two models do not collapse, their scaling behaviour is correctly captured by both models, as evident from the collapse of the profiles for each model.

The differences between the profiles (the extent of the log-law region and the value of the von Kármán constant) obtained using the two SGS models indicate that the SGS model has strong effects and could result in deviation from the Monin–Obukhov scaling. Therefore, it is unlikely that the Monin–Obukhov scaling of the LES mean velocity profile at heights greater than the first few grid points is a result of the boundary condition.

To examine the convective logarithmic friction law, we plot U_m/u_* in figure 6 as a function of $-L/h_0$ for the same LES runs. The value of the von Kármán constant for each model (the inverse of the slope) is obtained from figure 5 (0.35 and 0.55

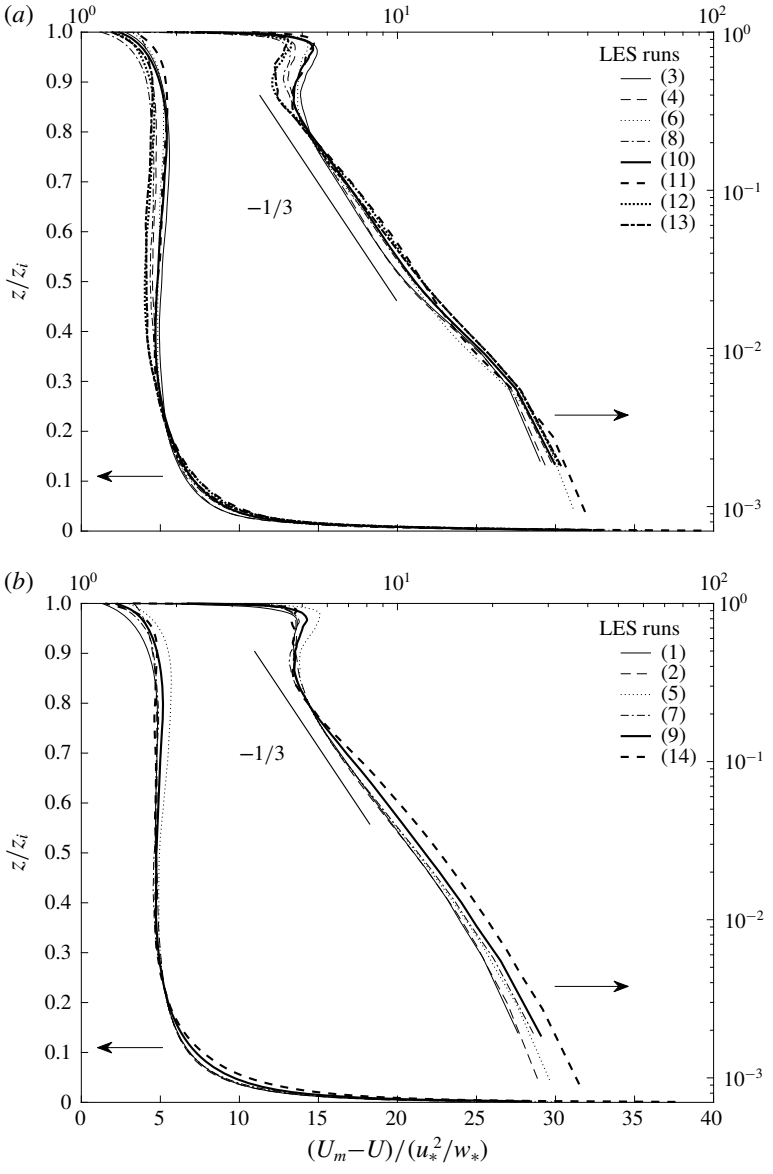

FIGURE 3. The mixed-layer velocity-defect profiles obtained from LES runs with several $-z_i/L$ values as shown in table (1) using the (*a*) Smagorinsky model and (*b*) Kosović model. The arrows indicate the ordinates that the curves correspond to.

for the Smagorinsky and Kosović models, respectively). In spite of the difference in the values of the von Kármán constant obtained, the data points for each SGS model follow the friction law well, indicating that the scaling laws predicted by LES are robust. Interestingly for some of the LES runs with large $-z_i/L$ values, although the log law is not present, the convective logarithmic friction law is followed, suggesting that the friction law is quite robust. Although the constants in the friction law obtained for the Smagorinsky and Kosović models are different, perhaps due to the different predicted u_* values, the scaling properties are correctly predicted by both models.

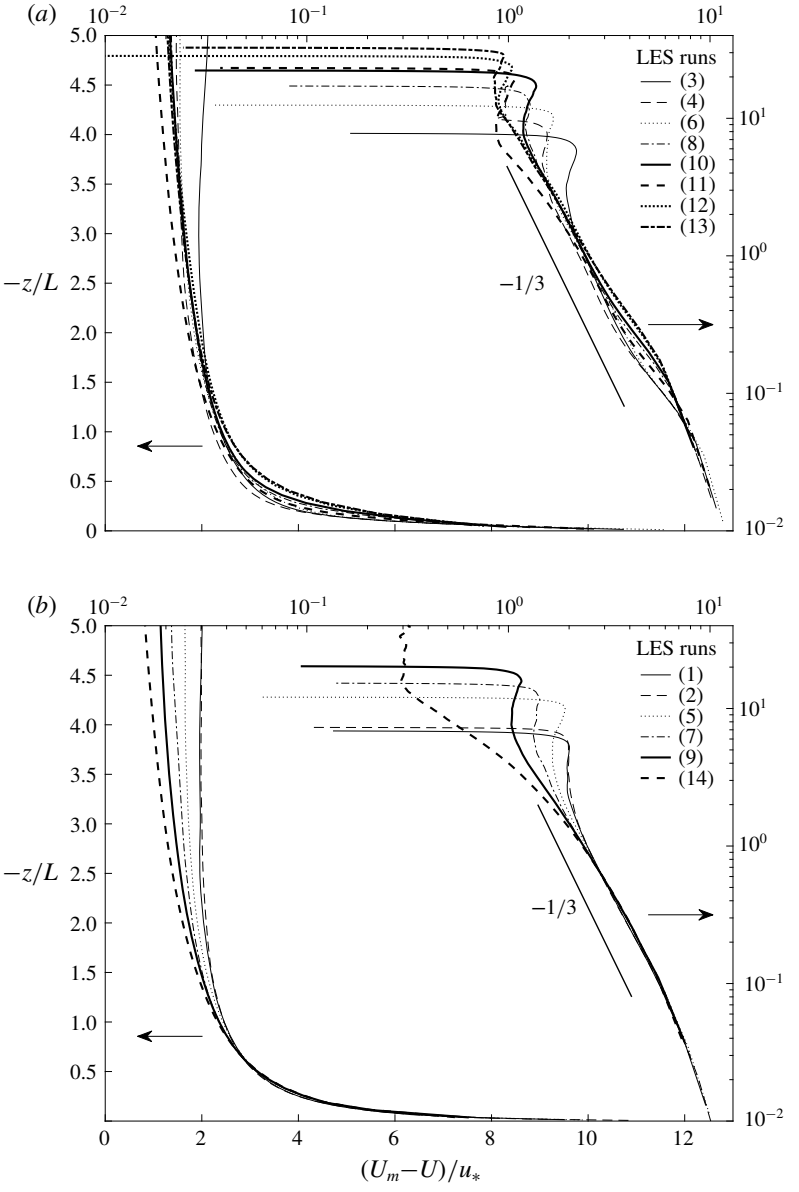

FIGURE 4. The surface-layer velocity-defect law profiles obtained from LES with several $-z_i/L$ values using the (*a*) Smagorinsky model and (*b*) Kosović model. The arrows indicate the ordinates that the curves correspond to.

4. Conclusions and discussion

In the present work we derived analytically the mean velocity profile in the convective atmospheric boundary layer that has Monin–Obukhov similarity ($-L \ll z_i$). It is part of a comprehensive analytical derivation of the MMO scaling properties of the surface-layer statistics, including the multi-point statistics (Tong & Ding 2019), one-point fluctuation statistics (Tong & Ding 2018), and the mean field (present study).

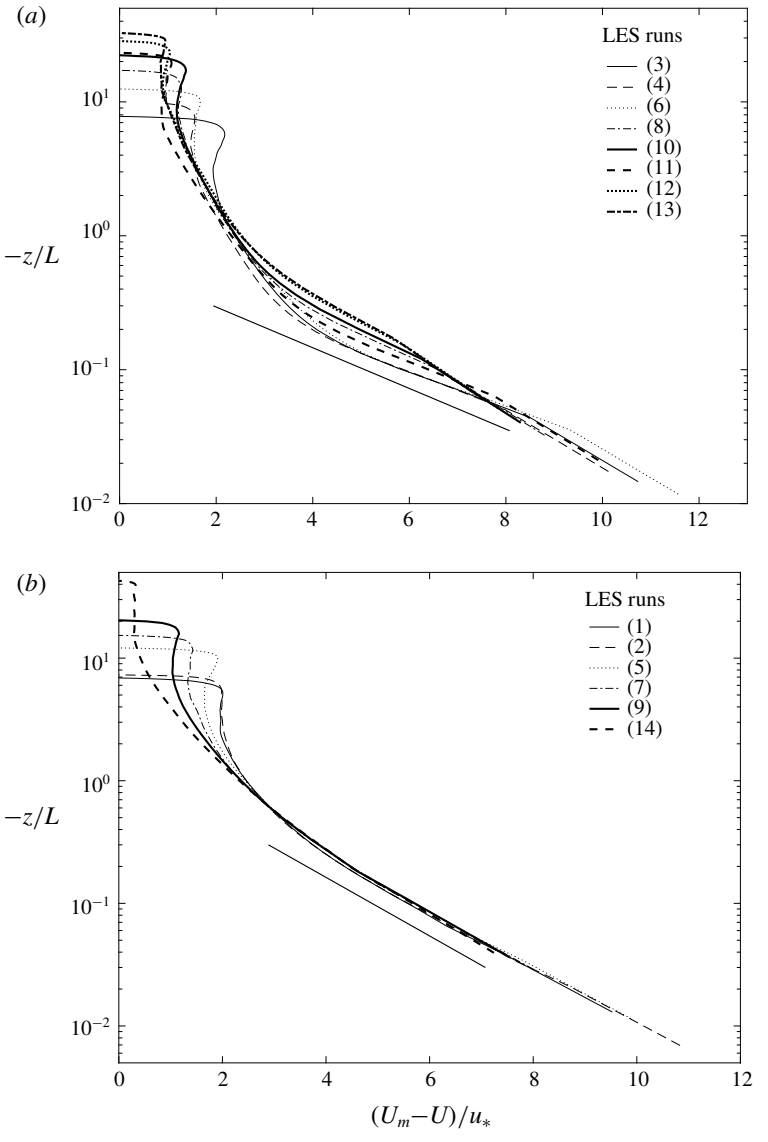

FIGURE 5. The surface-layer logarithmic law obtained from LES with several $-z_i/L$ values using the (*a*) Smagorinsky model and (*b*) Kosović model.

Note that the multi-point statistics cannot be predicted by MOST, while only some of the one-point fluctuation statistics can be predicted by MOST.

The shear-stress budget equations (2.1) and (2.2) and the mean momentum equations (2.3) and (2.4) are employed in the derivation. The scaling properties of the statistics in the shear-stress budget equations needed for the derivation are obtained using predictions based on MMO. Previous analysis (Tong & Ding 2019) and this work have shown that CBL is mathematically a singular perturbation problem. Therefore, we obtain the mean velocity profile using the method of matched asymptotic expansions.

The analysis shows that the Coriolis force results in jumps in the streamwise and cross-stream mean velocity components across the inversion layer, the former

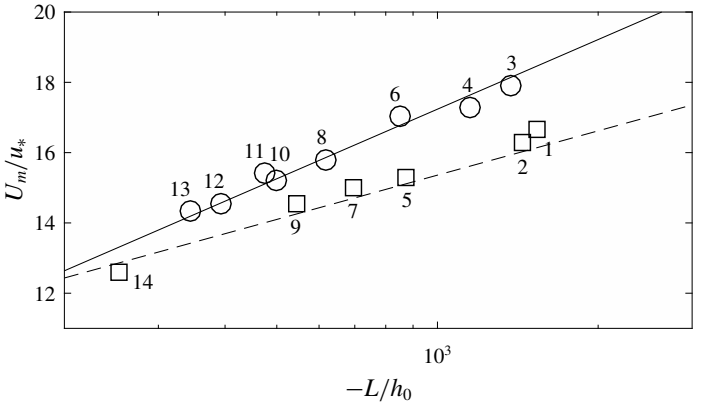

FIGURE 6. The convective logarithmic friction law obtained from LES with several $-z_i/L$ values using the Smagorinsky model (solid) and the Kosović model (dashed). The slope of the lines are obtained from figure 5.

corresponding to the cross-stream shear stress generated by the entrainment of the air above the inversion layer, and the latter corresponding to the streamwise pressure gradient driving the flow in the boundary layer. The effects of Earth's rotation on the shear-stress budget equations are of higher order and are neglected. The change in the direction of the mean velocity vector in the boundary layer due to Earth's rotation is much smaller than that across the inversion layer.

Three scaling layers are identified: the outer layer, which includes the mixed layer, the inner-outer layer and the inner-inner layer, which includes the roughness layer. There are two overlapping layers, the local-free-convection layer and the log layer, respectively. The analysis shows that in the outer layer the leading term, the streamwise mean-shear production, is zero, resulting in a leading term velocity equalling the mixed-layer mean velocity scale U_m (2.26). The second-order term is a velocity defect with a scale of $u_*(-z_i/L)^{-1/3}$, leading to the discovery of the mixed-layer velocity-defect law (2.20). In the inner-outer layer, the leading-order term is also zero, again leading to a leading-order mixed-layer mean velocity equalling U_m. The second-order term is also a velocity defect, but with a scale of u_*, leading to the discovery of the surface-layer velocity-defect law (2.46). Asymptotically matching the expansions in the outer and inner-outer layers resulting in the local-free-convection scaling for the U-component (2.57) and a Coriolis term with a $(-z/L)^{2/3}$ dependence for the V-component (2.64). The existence of the inner-outer layer limits the extent of the outer layer scaling to $z > -L$, instead of $z \gg h_o$ in the neutral ABL. Previous attempts to examine the velocity defect defined it incorrectly as $U - U_g$ instead of $U - U_m$. Furthermore, only one scale of velocity defect was found for both the inner-outer and the outer layers.

In the inner-inner layer, the zero leading-order mean-shear production leads to a zero leading-order mean velocity. Matching the expansions in the inner-outer and the inner-inner layer leads to a log law contribution (2.92).

A new friction law, the convective logarithmic friction law (2.95) is obtained by combining the log law in terms of the inner-outer and inner-inner variables and therefore is an exact leading-order result. It has the same form as the logarithmic friction law for a neutral boundary layer over a rough wall, but with the boundary layer height replaced by the Obukhov length. Intuitively this is because to the

leading-order the mean velocity near $z = -L$ is U_m. This friction law can have important implications to practical applications. The inverse of the von Kármán constant is obtained as the rate of change of U_m/u_* with respect to $\ln(-L/h_0)$. Previous geostrophic drag laws were obtained using approximation of the mean velocity and U_g instead of U_m.

The surface-layer velocity-defect law (2.46) provides important interpretations of the expressions for the velocity profile: equation (2.96) (Monin & Obukhov 1954) and (2.101) (Panofsky & Dutton 1984). The former is closer to the defect law, although this cannot be inferred from (2.101) without the knowledge of the defect law. The latter profile has the appearance of a modified law of the wall with an added dependence on $-z/L$. However, the defect law shows that the dependence of U/u_* on $-z/L$ actually comes entirely in the form of the velocity defect. Therefore, it is not a modified law of the wall. In addition, the fact that $U \to U_m$ when $z \to -L$ cannot be inferred from this profile. Thus, while this profile has the correct behaviour and is useful for practical applications, its origin and interpretation only become clear with the discovery of the surface-layer velocity-defect law. The surface-layer velocity-defect law also indicates that buoyancy effects reduce the extent of the law of the wall. In a convective boundary layer, it is only valid up to $z < -L$, i.e. it ceases to be valid as z approaches $-L$.

We note that for the CBL with $-L \sim z_i$ or $-L > z_i$, buoyancy does not introduce an inner-outer layer in the singular perturbation problem. Such a case can be analysed as a modified neutral boundary layer, which has a two layer structure. In addition, the surface layer does not obey Monin–Obukhov similarity. Therefore, the CBL with $-L \ll z_i$ (strong buoyancy) is structurally different from one with $-L \sim z_i$ or $-L > z_i$ (weak buoyancy).

In the present work we performed preliminary comparisons of the derived mean velocity profile to LES results. While the agreement is good, more comprehensive comparisons, especially with field measurements, are needed to further validate the prediction as well as to establish the values of the coefficients in the expansions. Preparations for a field campaign for this purpose are under way.

The predicted mean velocity profile, especially the two velocity-defect laws, has implications for applications where the mean velocity is important, such as transport of pollutants by the mean velocity in the boundary layer, wind turbine, aerodynamic loading on structures, etc. We note that it might be numerically more accurate to use the surface-layer velocity-defect law instead of (2.101) in practical applications. The convective logarithmic friction law can potentially be used to predict the surface stress in meso- and large-scale simulations.

The present work is an integral part of a comprehensive derivation of MMO scaling using first principles. In deriving the vertical velocity variance and temperature variance profiles in the CBL (Tong & Ding 2018), the scaling properties of the terms in the variance equations (derived using MMO) and the mean velocity gradient (provided by the present study) were used. The present study derives the scaling of the mean velocity. The scaling of the terms in the shear-stress and mean momentum equations (provided by MMO) was used. The results from these derivations are the solution of the set of simultaneous equations employed in the derivations, and are comprehensive MMO scaling properties.

The fact that multi-point statistics represent the complete surface-layer similarity, whereas one-point statistics do not, suggests that the similarity properties of these statistics are different in nature. Tong & Ding (2019) have shown that the surface-layer similarity of multi-point statistics results directly from that of the surface-layer eddies,

suggesting that the former is a fundamental similarity. The similarity of one-point statistics, on the other hand, results indirectly from that of the surface-layer eddies, and may involve additional aspects of the surface-layer dynamics (e.g. variance and mean momentum equations). It needs to be derived from the similarity properties of the multi-point statistics, and therefore is derived similarly.

Acknowledgements

We would like to acknowledge high-performance computing support from Cheyenne (doi:10.5065/D6RX99HX) provided by NCAR's Computational and Information Systems Laboratory, sponsored by the National Science Foundation. Clemson University is acknowledged for the generous allotment of compute time on Palmetto cluster. This work was supported by the National Science Foundation through grants no. AGS-1561190.

REFERENCES

ARYA, S. P. S. 1975 Geostrophic drag and heat transfer relations for the atmospheric boundary layer. *Q. J. R. Meteorol. Soc.* **101**, 147–161.

BLACKADAR, A. K. & TENNEKES, H. 1968 Asymptotic similarity in neutral barotropic planetary boundary layers. *J. Atmos. Sci.* **25**, 1015–1020.

BRASSEUR, J. G. & WEI, T. 2010 Designing large-eddy simulation of the turbulent boundary layer to capture law-of-the-wall scaling. *Phys. Fluids* **22**, 021303.

BROWN, R. A. 1973 On the atmospheric boundary layer: Theory and methods. *Arctic Ice Dynamics Joint Experiment Bulletin* **20**, 1–141.

BUSINGER, J. A. 1973 A note on free convection. *Boundary-Layer Meteorol.* **4**, 323–326.

BUSINGER, J. A., WYNGAARD, J. C., IZUMI, Y. & BRADLEY, E. F. 1971 Flux-profile relationships in the atmospheric surface layer. *J. Atmos. Sci.* **28**, 181–189.

CAUGHEY, S. J. & PALMER, S. G. 1979 Some aspects of turbulence structure through the depth of the convective boundary layer. *Q. J. R. Meteorol. Soc.* **105**, 811–827.

CLARKE, R. H. 1970*a* Observational studies in the atmospheric boundary layer. *Q. J. R. Meteorol. Soc.* **96**, 91–114.

CLARKE, R. H. 1970*b* Recommended methods for the treatment of the boundary layer in numerical models. *Austral. Met. Mag.* **18**, 51–73.

CLARKE, R. H. 1972 Discussion of 'observational studies in the atmospheric boundary layer'. *Q. J. R. Meteorol. Soc.* **98**, 234–235.

CSANADY, G. T. 1967 On the resistance law of a turbulent ekman layer. *J. Atmos. Sci.* **24**, 467–471.

DEARDORFF, J. W. 1973 An explanation of anomalously large Reynolds stresses within the convective planetary boundary layer. *J. Atmos. Sci.* **30**, 1070–1076.

GARRATT, J. R., WYNGAARD, J. C. & FRANCEY, R. J. 1982 Winds in the atmospheric boundary layer-prediction and observation. *J. Atmos. Sci.* **39**, 1307–1316.

GRACHEV, A. A., FAIRALL, C. W. & ZILITINKEVICH, S. S. 1997 Surface-layer scaling for the convection induced stress regime. *Boundary-Layer Meteorol.* **83**, 423–439.

KAIMAL, J. C. 1978 Horizontal velocity spectra in an unstable surface layer. *J. Atmos. Sci.* **35**, 18–24.

KAIMAL, J. C., WYNGAARD, J. C., IZUMI, Y. & COTÉ, O. R. 1972 Spectral characteristic of surface-layer turbulence. *Q. J. R. Meteorol. Soc.* **98**, 563–589.

VON KÁRMÁN, T. 1930 Mechanische Ähnlichkeit und Turbulenz. In *Proceedings of the Third International Congr. Applied Mechanics*, pp. 85–105. Stockholm.

KAZANSKI, A. B. & MONIN, A. S. 1960 A turbulent regime above the surface atmospheric layer. *Izv. Acad. Sci., USSR, Geophys. Ser.* **1**, 110–112.

KOSOVIĆ, B. 1997 Subgrid-scale modelling for the large-eddy simulation of high-Reynolds-number boundary layer. *J. Fluid Mech.* **336**, 151–182.

LETTAU, H. H. 1959 Wind profile, surface stress and geostrophic drag coefficients in the atmospheric surface layer. *Adv. Geophys.* **6**, 241–257.

LILLY, D. K. 1967 The representation of small-scale turbulence in numerical simulation experiments. In *Proceedings of the IBM Scientific Computing Symp. on Environ. Sci.* (ed. H. H. Goldstine), pp. 195–210. IBM.

LILLY, D. K. 1968 Models of cloud-topped mixed layers under a strong inversion. *Q. J. R. Meteorol. Soc.* **94**, 292–309.

LUMLEY, J. L. & PANOFSKY, H. A. 1964 *The Structure of Atmospheric Turbulence*, Interscience Monographs and Texts in Physics and Astronomy, vol. 12. Interscience.

MASON, P. J. & THOMSON, D. J. 1992 Stochastic backscatter in large-eddy simulations of boundary layers. *J. Fluid Mech.* **242**, 51–78.

MILES, N. L., WYNGAARD, J. C. & OTTE, M. J. 2004 Turbulent pressure statistics in the atmospheric boundary layer from large-eddy simulation. *Boundary-Layer Meteorol.* **113**, 161–185.

MILLIKAN, C. B. 1938 A critical discussion of turbulent flows in channels and circular tubes. In *Proceedings of the Fifth International Conference Appl. Mech*. John Wiley and Sons.

MOENG, C.-H. 1984 A large-eddy simulation model for the study of planetary boundary-layer turbulence. *J. Atmos. Sci.* **41**, 2052–2062.

MOENG, C. H. & WYNGAARD, J. C. 1988 Spectral analysis of large-eddy simulations of the convective boundary layer. *J. Atmos. Sci.* **45**, 3573–3587.

MONIN, A. S. & OBUKHOV, A. M. 1954 Basic laws of turbulent mixing in the ground layer of the atmosphere. *Trans. Inst. Teoret. Geofiz. Akad. Nauk SSSR* **151**, 163–187.

OBUKHOV, A. M. 1946 Turbulence in the atmosphere with inhomogeneous temperature. *Trans. Inst. Teoret. Geofiz. Akad. Nauk SSSR* **1**, 95–115.

OTTE, M. J. & WYNGAARD, J. C. 2001 Stably stratified interfacial-layer turbulence from large-eddy simulation. *J. Atmos. Sci.* **58**, 3424–3442.

PANOFSKY, H. A. & DUTTON, J. 1984 *Atmospheric Turbulence*. Wiley-Interscience.

PANTON, R. L. 2005 Review of wall turbulence as described by composite expansions. *Appl. Mech. Rev.* **58**, 1–36.

PRANDTL, L. 1925 Bericht Über die Entstehung der Turbulenz. *Z. Angew. Math. Mech.* **5**, 136–139.

SMAGORINSKY, J. 1963 General circulation experiments with the primitive equations: I. The basic equations. *Mon. Weath. Rev.* **91**, 99–164.

SPALART, P. R., MOSER, R. D. & ROGERS, M. M. 1991 Spectral methods for the Navier–Stokes equations with one infinite and 2 periodic directions. *J. Comput. Phys.* **96**, 297–324.

SULLIVAN, P. P., MCWILLIAMS, J. C. & MOENG, C.-H. 1994 A subgrid-scale model for large-eddy simulation of planetary boundary-layer flows. *Boundary-Layer Meteorol.* **71**, 247–276.

SULLIVAN, P. P., MCWILLIAMS, J. C. & MOENG, C.-H. 1996 A grid nesting method for large-eddy simulation of planetary boundary-layer flows. *Boundary-Layer Meteorol.* **80**, 167–202.

SYKES, R. I., HENN, D. S. & LEWELLEN, W. S. 1993 Surface-layer description under free-convection conditions. *Q. J. R. Meteorol. Soc.* **119**, 409–421.

TONG, C. & DING, M. 2018 Monin-Obukhov similarity and local-free-convection scaling in the atmospheric boundary layer using matched asymptotic expansions. *J. Atmos. Sci.* **75**, 3691–3701.

TONG, C. & DING, M. 2019 Multi-point Monin-Obukhov similarity in the convective atmospheric surface layer using matched asymptotic expansions. *J. Fluid Mech.* **864**, 640–669.

TONG, C. & NGUYEN, K. X. 2015 Multipoint monin-obukhov similarity and its application to turbulence spectra in the convective atmospheric surface layer. *J. Atmos. Sci.* **72**, 4337–4348.

TOWNSEND, A. A. 1976 *The Structure of Turbulent Shear Flows*. Cambridge University Press.

WYNGAARD, J. C. 2010 *Turbulence in the Atmosphere*. Cambridge University Press.

WYNGAARD, J. C. & COTÉ, O. R. 1971 The budgets of turbulent kinetic energy and temperature variance in the atmospheric surface layer. *J. Atmos. Sci.* **28**, 190–201.

WYNGAARD, J. C., COTÉ, O. R. & IZUMI, Y. 1971 Local free convection, similarity, and the budgets of shear stress and heat flux. *J. Atmos. Sci.* **28**, 1171–1182.

ZILITINKEVICH, S. S. 1969 On the computation of the basic parameters of the interaction between the atmosphere and the ocean. *Tellus* **21**, 17–24.

ZILITINKEVICH, S. S. 1975 Resistance laws and prediction equations for the depth of the planetary boundary layer. *J. Atmos. Sci.* **32**, 741–752.

ZILITINKEVICH, S. S. & CHALIKOV, D. V. 1968 The laws of resistance and of heat and moisture exchange in the interaction between the atmosphere and an underlying surface. *Izv. Atmos. and Ocean Phys.* **4**, 438–441.

ZILITINKEVICH, S. S. & DEARDORFF, J. W. 1974 Similarity theory for the planetary boundary layer of time-dependent height. *J. Atmos. Sci.* **31**, 1449–1452.

ZILITINKEVICH, S. S., FEDOROVICH, E. E. & SHABALOVA, M. V. 1992 Numerical model of a non-steady atmospheric planetary boundary layer, based on similarity theory. *Boundary-Layer Meteorol.* **59**, 387–411.

ZILITINKEVICH, S. S., HUNT, J. C. R., ESAU, I. N., GRACHEV, A. A., LALAS, D. P., AKYLAS, E., TOMBROU, M., FAIRALL, C. W., FERNANDO, H. J. S., BAKLANOV, A. A. *et al.* 2006 The influence of large convective eddies on the surface-layer turbulence. *Q. J. R. Meteorol. Soc.* **132**, 1423–1456.

ZILITINKEVICH, S. S., LAIKHTMAN, D. L. & MONIN, A. S. 1967 Dynamics of the atmospheric boundary layer. *Izv. Atmohs. and Ocean Phys.* **3**, 170–191.